

Direction Finding with Sparse Subarrays: Design, Algorithms and Analysis

Wesley S. Leite, Rodrigo C. de Lamare, Yuriy Zakharov, Wei Liu and Martin Haardt

Abstract—This paper proposes design techniques for partially-calibrated sparse linear subarrays and algorithms to perform direction-of-arrival (DOA) estimation. First, we introduce array architectures that incorporate two distinct array categories, namely type-I and type-II arrays. The former breaks down a known sparse linear geometry into as many pieces as we need, and the latter employs each subarray such as it fits a preplanned sparse linear geometry. Moreover, we devise two Direction of Arrival (DOA) estimation algorithms that are suitable for partially-calibrated array scenarios within the coarray domain. The algorithms are capable of estimating a greater number of sources than the number of available physical sensors, while maintaining the hardware and computational complexity within practical limits for real-time implementation. To this end, we exploit the intersection of projections onto affine spaces by devising the Generalized Coarray Multiple Signal Classification (GCA-MUSIC) in conjunction with the estimation of a refined projection matrix related to the noise subspace, as proposed in the GCA root-MUSIC algorithm. An analysis is performed for the devised subarray configurations in terms of degrees of freedom, as well as the computation of the Cramèr-Rao Lower Bound for the utilized data model, in order to demonstrate the good performance of the proposed methods. Simulations assess the performance of the proposed design methods and algorithms against existing approaches.

Index Terms—Direction-of-Arrival Estimation, Sparse Linear Array, MUSIC, Non-Uniform Linear Arrays

I. INTRODUCTION

OVER the past decade, a primary focus in sensor array processing has been the advancement of increasingly accurate and efficient techniques for direction of arrival (DOA) estimation. This particular problem has its own fundamental importance and is strongly related to the fields of radar, sonar, wireless communications, seismology, and radio astronomy. Therefore, the problem is of great interest for several scientific research domains and practical applications exploiting sensor array technologies [1].

A. Prior and Related Works

Recently, many research works have focused on the particular problem of underdetermined DOA estimation [2]–[4]. This problem consists of the determination of directions of more signal sources than the number of physical sensors in the array. Other works also focus on the reduction of hardware complexity, which encompasses hardware costs and energy-saving capabilities that are closely related to system

This work was supported by FAPERJ, CNPq and FAPESP. The work of Y. Zakharov was supported in part by U.K. EPSRC under Grant P/V009591/1. W. S. Leite, and R. C. de Lamare are with Department of Electrical Engineering, PUC-Rio, Rio de Janeiro 22451-900, Brazil. R. C. de Lamare and Y. Zakharov are with the School of Physics, Engineering and Technology, University of York, York, UK. W. Liu is with Department of Electrical and Electronic Engineering, The Hong Kong Polytechnic University, Kowloon, Hong Kong. Martin Haardt is with the Communications Research Laboratory, Ilmenau University of Technology, Germany (e-mail: wesleysouzaleite@gmail.com, delamare@puc-rio.br, yury.zakharov@york.ac.uk, wliu.eee@gmail.com, martin.haardt@tu-ilmenau.de).

operational costs and portability. The standard approach to DOA estimation employs a coherent sensor array, where the RF chains associated with sensors are connected to the same local oscillator and the intersensor distance is perfectly known (the array manifold is known), as well as the propagation channel mismatches. This approach is expensive and may be difficult to implement in many real-world situations, especially for large aperture arrays [5], [6].

A possible solution to this problem is to divide the whole array into subarrays and approach the task in one of two different ways: i) pre-process the subarray data separately and forward the processing results to a central processing unit (CPU - non-coherent processing); or ii) compensate for the unknown parameters that are needed for coherent processing by estimating them. For example, one can develop techniques to estimate the phase shifts between the steering vectors of the subarrays. Those phase shifts can be due to unknown intersubarray distances, lack of proper synchronization in time (non-coherent arrays), and unknown propagation channel mismatches (fades) [7].

In [8], a new method based on a convex optimization formulation derived from a bilinear arrangement and a convex relaxation procedure was developed. The authors estimate the phase shifts between the subarrays and then use the corrected data model to estimate the DOAs using the well-known sparse signal processing formulation presented in [9]. However, this method was developed for a single snapshot scenario and has a prohibitive computational complexity for most practical online processing scenarios. Moreover, in general it is not capable of estimating more sources than the number of physical sensors.

In [10], an approach for quasi-stationary signals was proposed, relying on the vectorization operator to build up a full-rank effective array manifold. This method was modified to deal with stationary signals through the introduction of a subspace-based algorithm known as Spatial Smoothing Multiple Signal Classification (SS-MUSIC) [2], [3] that performs spatial smoothing on the vectorized model, in the context of coherent (fully calibrated) arrays, and assumes uncorrelated sources. The boundaries of the algorithm performance were established later on in [11].

In [5], a decentralized, non-coherent DOA estimation algorithm was introduced based on the method of Projection onto Convex Sets (POCS) to compute a global estimate with the MUSIC algorithm. This strategy, subsequently referred to as G-MUSIC in Section VI, is a generalization of MUSIC. Notwithstanding its advantages, the algorithm possesses certain limitations. It was not explicitly engineered to deal with sparse arrays, although it remains compatible at some degree with such configurations. Moreover, its capability to estimate the number of sources is inherently constrained by the total number of sensors in each subarray through a linear relationship. In [12], a sparse recovery approach for DOA estimation in partly calibrated arrays that uses mixed nuclear norm and l_1 -norm minimization was introduced. Despite its

superior performance, it relies on iterative optimization, which is costly for some applications.

More recently, two novel subarray algorithms have been presented in [13]. The first one relies on a non-convex optimization framework, which is very costly and necessitates the initiation from a feasible point. Furthermore, it does not guarantee convergence to a global minimum, thus making it a potentially unreliable strategy. In contrast, the second algorithm, involving a procedure labelled as the SPICE algorithm, uses a convex optimization with guaranteed convergence, although it is unsuitable for real-world scenarios.

Thus, we note that there is a gap for efficient methods that can employ sparse arrays in partially-calibrated scenarios, while also addressing the underdetermined DOA estimation problem in a practical manner. The aim of this study is to present cost-effective approaches to this problem through sparse subarray design, as well as a signal processing strategy to estimate more sources than sensors in each subarray. Thus, we can devise cost-effective methods to estimate as many sources as possible using sparse subarrays, while reducing hardware and computational costs through a partially-calibrated scheme.

B. Contributions

In this work, we present design techniques for partially-calibrated sparse linear subarrays and algorithms to perform DOA estimation. First, we detail array architectures that incorporate two distinct array categories, namely type-I and type-II arrays, whose preliminary results appeared in [14]. The former breaks down a known sparse linear geometry into as many pieces as we need, and the latter employs each subarray such as it fits a preconceived sparse linear geometry. Moreover, we devise two DOA estimation algorithms that are suitable for partially-calibrated array scenarios within the coarray domain. In particular, we exploit the intersection of projections onto affine spaces and derive the Generalized Coarray Multiple Signal Classification (GCA-MUSIC), whose preliminary results and description were reported in [15], and then we develop a root version of GCA-MUSIC that is denoted as the GCA root-MUSIC (GCA-rMUSIC) algorithm. The GCA-MUSIC and GCA-rMUSIC algorithms are suitable for scenarios within the coarray domain, allow the estimation of more sources than sensors in each subarray by handling the underdetermined case and do not rely on potentially costly iterative schemes or non-convex optimization. An analysis is performed for the proposed subarray configurations in terms of degrees of freedom. Moreover, we derive the Cramèr-Rao Lower Bound (CRLB) and its associated Fisher Information Matrices for the adopted data model. Simulations assess the performance of the proposed design methods and algorithms against existing approaches.

Paper structure: In Section II, the data model is introduced. In Section III, the type-I and type-II sparse arrays are presented. In Section IV, the proposed GCA-MUSIC and GCA-rMUSIC algorithms are derived. A complexity analysis for both algorithms is performed in Section V, along with the properties of type-I and type-II arrays, as well as the CRLB. Numerical results in Section VI show the algorithms' and arrays' ability in identifying the sources, whereas Section VII draws the conclusions.

Notation: The symbols \mathbb{S} , a , \mathbf{a} and \mathbf{A} refer to sets, scalars, column vectors and matrices, respectively. $[a]$ means the set $\{1, \dots, a\}$. $|\mathbb{A}|$ denotes the cardinality of the set \mathbb{A} . The symbols $\mathcal{R}(\mathbf{A})$ and $\mathcal{N}(\mathbf{A})$ are the range and null space of matrix \mathbf{A} , respectively. \mathbf{I}_M is the $M \times M$ identity matrix. $[a]$ means the set $\{1, \dots, a\}$. $\text{blkdiag}(\cdot)$ is the block diagonal matrix, whereas $\text{colspan}(\mathbf{A})$ represents the column space of \mathbf{A} .

II. SYSTEM MODEL AND PROBLEM STATEMENT

The received signal model for a multiple measurements scenario is given by

$$\mathbf{x}_S(t) = \tilde{\mathbf{V}}(\boldsymbol{\theta})\tilde{\mathbf{H}}\mathbf{s}(t) + \mathbf{n}_S(t), \quad t \in [T] \quad (1)$$

where

$$\begin{aligned} \tilde{\mathbf{V}}(\boldsymbol{\theta}) &= [\mathbf{V}(\boldsymbol{\theta}_1), \dots, \mathbf{V}(\boldsymbol{\theta}_D)] \in \mathbb{C}^{N \times LD} \\ \mathbf{V}(\boldsymbol{\theta}_d) &= \text{blkdiag}(\mathbf{a}_1(\boldsymbol{\theta}_d), \dots, \mathbf{a}_L(\boldsymbol{\theta}_d)) \in \mathbb{C}^{N \times L} \\ \tilde{\mathbf{H}} &= \text{blkdiag}(\mathbf{h}_1, \dots, \mathbf{h}_D) \in \mathbb{C}^{LD \times D} \\ \mathbf{h}_d &= [1, h_{2d}, h_{3d}, \dots, h_{Ld}]^T \in \mathbb{C}^{L \times 1} \end{aligned} \quad (2)$$

for $l \in \{1, \dots, L\}$ and $t \in \{1, \dots, T\}$, where L is the number of subarrays and T is the number of snapshots. The vector $\mathbf{x}_S(t) \in \mathbb{C}^N$ represents the array received signal, $\mathbf{s}(t) \in \mathbb{C}^D$ is the source signal vector, and $\mathbf{n}_S(t) \in \mathbb{C}^N$ is the array noise vector. There are D impinging sources with normalized directions given by $\boldsymbol{\theta} \in [-1, 1]^D$ (sine of DOAs). The noise and the source signals are drawn from a circularly complex multivariate Gaussian distribution. The noise is spatially and temporally white, and the noise and sources are uncorrelated. The vector \mathbf{h}_d contains the calibration parameters associated with all the subarrays (first subarray as reference) for the d -th direction, and $[\mathbf{a}_l(\boldsymbol{\theta})]_k = \exp(j\pi n_k \boldsymbol{\theta})$ is the k -th element of the steering vector of the l -th subarray, $n_k \in \mathbb{S}_l$ is the k -th sensor position as an integer multiple of the minimum intersensor distance, the set of integers \mathbb{S}_l and N_l define the sensor locations and number of sensor elements of the l -th subarray, respectively.

The received signal in (1) can alternatively be rewritten as

$$\begin{aligned} \mathbf{x}_S(t) &= [\mathbf{V}(\boldsymbol{\theta}_1)\mathbf{h}_1, \dots, \mathbf{V}(\boldsymbol{\theta}_D)\mathbf{h}_D] \mathbf{s}(t) + \mathbf{n}_S(t) \\ &= \begin{bmatrix} \mathbf{A}_1(\boldsymbol{\theta}) \\ \mathbf{A}_2(\boldsymbol{\theta})\mathbf{G}_2 \\ \vdots \\ \mathbf{A}_L(\boldsymbol{\theta})\mathbf{G}_L \end{bmatrix} \mathbf{s}(t) + \mathbf{n}_S(t) \end{aligned} \quad (3)$$

where $\mathbf{A}_l(\boldsymbol{\theta}) \in \mathbb{C}^{N_l \times D}$ is the l -th calibrated subarray manifold¹ with geometry defined by the set of integers \mathbb{S}_l , and $\mathbf{G}_l = \text{diag}([h_{1l}, \dots, h_{Ll}])$. \mathbf{G}_1 is the identity matrix of order D , which is why it is not included in (3). The array received signal $\mathbf{x}_S(t)$ can be partitioned as

$$\mathbf{x}_S(t) = [\mathbf{x}_{S_1}^T(t), \mathbf{x}_{S_2}^T(t), \dots, \mathbf{x}_{S_L}^T(t)]^T \quad (4)$$

From that, it is clear that each subarray received signal in (4) can be rewritten as

$$\mathbf{x}_{S_l}(t) = \mathbf{A}_l(\boldsymbol{\theta})\mathbf{G}_l\mathbf{s}(t) + \mathbf{n}_{S_l}(t) \quad (5)$$

¹Notice that the subarrays are calibrated; however, the whole array is only partially calibrated because the differences in calibration parameters between different subarrays are unknown (e.g., their relative distances).

$\mathbf{x}_{\mathbb{S}_l}(t) \in \mathbb{C}^{N_l}$ is the l -th subarray received signal snapshot, and $\mathbf{n}_{\mathbb{S}_l}(t)$ is the subarray noise vector measurement². If we calculate the covariance matrix for each of the subarray data, we have

$$\begin{aligned} \mathbf{R}_{\mathbb{S}_l} &= \mathbf{A}_l(\boldsymbol{\theta})\mathbf{G}_l\mathbf{R}_s\mathbf{G}_l^H\mathbf{A}_l^H(\boldsymbol{\theta}) + \sigma_n^2\mathbf{I}_{N_l} \\ &= \mathbf{A}_l(\boldsymbol{\theta})\mathbf{R}_s\mathbf{A}_l^H(\boldsymbol{\theta}) + \sigma_n^2\mathbf{I}_{N_l} \end{aligned} \quad (6)$$

where σ_n^2 is the noise variance, $\mathbf{R}_{\mathbb{S}_l}$ is the received signal covariance matrix of the l -th subarray. In (6) we have used the fact that each calibration parameter h_{ld} has a unitary module, according to what follows:

$$\begin{aligned} \mathbf{G}_l\mathbf{R}_s\mathbf{G}_l^H &= \text{diag}(h_{l1}p_1h_{l1}^*, \dots, h_{lD}p_1h_{lD}^*) \\ &= \text{diag}(|h_{l1}|^2p_1, \dots, |h_{lD}|^2p_1) \\ &= \text{diag}(\mathbf{p}) \\ &= \mathbf{R}_s \end{aligned} \quad (7)$$

where $\mathbf{p} = [\sigma_1^2, \dots, \sigma_D^2]$ contains the powers of the sources.

Remark 1: This demonstrates that, although the subarrays are uncalibrated relative to each other, the covariance matrix of each subarray does not depend on the calibration parameters. Conversely, while the subarrays are individually calibrated, the full array remains uncalibrated. We refer to this condition as a ‘‘partially-calibrated array’’.

By vectorizing (6), we arrive at

$$\mathbf{z}_{\mathbb{S}_l} = (\mathbf{A}_{\mathbb{S}_l}^*(\boldsymbol{\theta}) \circ \mathbf{A}_{\mathbb{S}_l}(\boldsymbol{\theta})) \mathbf{p} + \sigma_n^2 \bar{\mathbf{i}}, \quad (8)$$

where \circ denotes the Khatri-Rao product, $\bar{\mathbf{i}} = [\mathbf{e}_{N_l}^T, \dots, \mathbf{e}_{N_l}^T]^T$ is the vectorization of the identity matrix, and \mathbf{e}_i is the i -th canonical basis vector (all-zeros vector except for a 1 at the i -th position). To simplify the equations, we will assume N/L sensors for each subarray, where $N = \sum_{l=1}^L N_l$ is the total number of sensors. By removing the repeated rows in $\mathbf{A}_{\mathbb{S}_l}^*(\boldsymbol{\theta}) \circ \mathbf{A}_{\mathbb{S}_l}(\boldsymbol{\theta})$ after their first occurrence (mirroring the operation in $\mathbf{z}_{\mathbb{S}_l}$ and $\bar{\mathbf{i}}$)³ and sorting the virtual sensor (coarray) elements in ascending order, we have

$$\mathbf{x}_{\mathbb{D}_l} = \mathbf{A}_{\mathbb{D}_l}(\boldsymbol{\theta})\mathbf{p} + \sigma_n^2\mathbf{i}, \quad (9)$$

where \mathbb{D}_l denotes the difference coarray set associated with the l -th subarray, $[\mathbf{A}_{\mathbb{D}_l}(\boldsymbol{\theta})]_{m,d} = \exp(j\pi n_m \theta_d)$ with $n_m \in \mathbb{D}_l$, $\mathbf{x}_{\mathbb{D}_l} \in \mathbb{C}^{|\mathbb{D}_l|}$ is the l -th coarray received signal and $\mathbf{i} \in \{0, 1\}^{|\mathbb{D}_l|}$ is an all-zero vector with the exception of a 1 in its half position (element $(|\mathbb{D}_l| + 1)/2$).

The problem of interest consists in estimating the source directions $\boldsymbol{\theta}$ from the pre-processed data in model (9).

III. SPARSE SUBARRAY DESIGN

There are many ways to perform the design of a sensor array that consists of subarrays. For example, one could rely on the split of a hypothetical geometry into smaller parts such that the aperture of the original array is greater than or equal to the sum of the apertures of the subarrays. The inequality instead of equality only comes from the fact that

²To simplify the equations, we assume equal SNRs across all subarrays, thereby standardizing the noise levels. Considering subarrays with differing SNRs represents a potential avenue for future research.

³In practice, with finite data sample, we average the repeated elements in $\mathbf{z}_{\mathbb{S}_l}$ instead of keeping only the first element. This gives a more accurate estimate of the statistic for this specific covariance lag.

the subarrays are separated by a distance of at least one unit of intersensor spacing. This is called a type-I subarray that is formally defined next.

Definition 1 (Type-I Sparse Linear Array): A type-I Sparse Linear Array (type-I SLA) corresponds to an array of pre-defined sparse linear geometry \mathbb{S} . The subsets defining the subarray geometries are generated from partitions $\mathbb{S}_l \subset \mathbb{S}$ such that if $s \in \mathbb{S}_i$ and $f \in \mathbb{S}_j$, $i < j$, then $s < f$.

The second most intuitive way of generating an array from subarrays would be to take subarrays with a predefined geometry and combine them to generate an array of a given aperture. This configuration is what we refer to as a type-II array. Type-II arrays are assumed to exhibit the same geometric pattern, i.e., the parent array consists of a union of subarrays with the same geometry. In what follows, we establish the formal definition.

Definition 2 (Type-II Sparse Linear Array): A type-II Sparse Linear Array (type-II SLA) corresponds to a union of subarrays with predefined sparse linear geometries \mathbb{S}_l (partitions of the array geometry \mathbb{S}). The set \mathbb{S}_1 defines the reference subarray. The remaining subarrays are derived from \mathbb{S}_1 through $\mathbb{S}_i = \mathbb{S}_{i-1}^{\Delta_{i-1}}$, where Δ_{i-1} is a translation factor for all the elements of \mathbb{S}_{i-1} and is given by $\Delta_{i-1} = \mu + \kappa_{i-1}$, where μ is the normalized distance between subarrays (in terms of integer multiples of d , that represents the minimum intersensor spacing) and κ_{i-1} is the aperture of the $(i-1)$ -th subarray.

Since all subarrays are translated versions of the reference subarray, characterized only by a linear translation factor, it follows that for any $i = 2, \dots, L$, the relationship $\kappa_{i-1} = \kappa_i$ holds in this case, indicating that the subarrays share identical sensors placement, except for a translation factor. However, we highlight that the definition can be easily extended for non-identical subarrays.

In what follows, we consider that the sets \mathbb{S} and \mathbb{S}_l have cardinality N and N_l , respectively, i.e., $|\mathbb{S}| = N$ and $|\mathbb{S}_l| = N_l$ and also $N = \sum_{l=1}^L N_l$. The definitions in both cases restrict the subarrays such that they obey the following rules: i) they do not share any sensors (partitions are pairwise disjoint); ii) they are colinear; and iii) the array is given by the union of the subarrays ($\mathbb{S} = \bigcup_{l=1}^L \mathbb{S}_l$). Note that the constraint $N_l = N/L$ (i.e., $\kappa_1 = \dots = \kappa_L = \kappa$) $\forall l \in [L]$, implies that the subarrays used to generate type-II SLAs are multiple invariant [16].

The key difference between these sparse array definitions is that for type-I SLAs the subarrays are generated by splitting an array with a predefined sparse geometry. On the other hand, for type-II SLA, the array is generated by a union of sparse linear subarrays with a predefined geometry.

Next, we define the difference coarray set, as well some other definitions that are important for the discussion that follows.

Definition 3: (Difference Coarray Set - \mathbb{D}) The difference coarray set represented by \mathbb{D} is a set associated with the sensor positions \mathbb{S} through

$$\mathbb{D} \triangleq \{n_1 - n_2 \mid (n_1, n_2) \in \mathbb{S}^2\} \quad (10)$$

arranged in ascending order and without repetition of elements.

Definition 4: (Degrees of Freedom - DoF) The number of DoF of a geometry specified by \mathbb{S} is the cardinality of its difference coarray set. Then,

$$\text{DoF} \triangleq |\mathbb{D}| \quad (11)$$

Definition 5: (Central Difference Coarray Consecutive Set - \mathbb{U}) The central difference coarray consecutive set, denoted by \mathbb{U} , associated with a difference coarray set \mathbb{D} is the set

$$\mathbb{U} = \{0\} \cup \{\pm [m]\} \quad (12)$$

arranged in ascending order and without any repetition of elements, such that m is chosen to maximize the cardinality of \mathbb{U} with $\mathbb{U} \subseteq \mathbb{D}$.

Definition 6: (Uniform Degrees of Freedom - UDoF) The number of Uniform DoF, denoted by UDoF, of a geometry specified by \mathbb{S} , is the cardinality of its central difference coarray consecutive set (\mathbb{U}), i.e.,

$$\text{UDoF} \triangleq |\mathbb{U}| \quad (13)$$

Let us now consider a well-known sparse linear geometry: the minimum redundancy array (MRA) [17]. The MRA is designed to minimize the number of pairs of physical sensors with the same position difference under the restriction that the associated difference coarray set is *hole-free*, which means that there are no missing lags in its covariance matrix.

To illustrate the concepts of type-I and type-II arrays, consider the sparse geometry defined by the set $\mathbb{S}^{\text{MRA}} = \{0, 1, 3, 6, 13, 20, 27, 31, 35, 36\}$, which corresponds to a MRA with $N = 10$ sensors. We adopt $L = 2$ subarrays. The corresponding type-I array is the original array itself, i.e., $\mathbb{S}_1^{\text{I-MRA}} = \mathbb{S}^{\text{MRA}}$, for an intersubarray displacement equal to $\mu = (20 - 13) = 7$ and its subarrays are given by $\mathbb{S}_1^{\text{I-MRA}} = \{0, 1, 3, 6, 13\}$ and $\mathbb{S}_2^{\text{I-MRA}} = \{20, 27, 31, 35, 36\}$. On the other hand, consider two MRAs with $N = 5$ sensors each given by $\mathbb{S}_1^{\text{II-MRA}} = \{0, 1, 4, 7, 9\}$ and $\mathbb{S}_2^{\text{II-MRA}} = \mathbb{S}_1^{\Delta_1, \text{II-MRA}} = \{10, 11, 14, 17, 19\}$, with translation factor $\Delta_1 = 1 + (9 - 0) = 10$. Thus, $\mathbb{S}^{\text{MRA}} = \mathbb{S}_1^{\text{I-MRA}} \neq \mathbb{S}_2^{\text{II-MRA}}$. For didactic purposes, Figure 1 shows a graphical representation of arrays in this example.

Before we proceed, it is worth discussing two additional sparse linear geometries, because they will be referred to later in the text: the two-level nested array (NAQ2) [3] and the Second-Order Super Nested Array (SNAQ2) [4].

The so-called n -th level nested array (NAQ n) was first introduced in [3]. The discussion is restricted here to the two-level nested array (NAQ2). The design rule (positioning procedure) described by \mathbb{S} is given by

$$\mathbb{S} = \{n, n = 0, 1, \dots, N_1 - 1\} \cup \{n(N_1 + 1) - 1, n = 1, 2, \dots, N_2\} \quad (14)$$

The total number of sensors is $N = N_1 + N_2$. Two of its fundamental properties are: a) hole free difference coarray ($\mathbb{D} = \mathbb{U}$); and b) the DoF/UDoF are given by $\text{DoF} = \text{UDoF} = 2N_2(N_1 + 1) - 1$. From that, notice that there are $\mathcal{O}(N_1 N_2)$ available DoF for arrays with only $N_1 + N_2$ sensors. The fact that NAQ2 structures have no holes in its coarray is a desired property for covariance matrix based algorithms, especially when spatial smoothing techniques are employed. The geometry SNAQ2 has the same filled coarray as NAQ2 with the advantage of reduced mutual electromagnetic coupling. Lastly, we also introduce the so-called weight function.

Definition 7 (Weight Function - $w(m)$): The weight function is an application

$$w : \mathbb{Z} \rightarrow \{0\} \cup \{\pm [N]\} \quad (15)$$

such that

$$w(m) = \begin{cases} |\mathbb{M}(m)| & \text{if } m \in \mathbb{D} \\ 0 & \text{otherwise} \end{cases} \quad (16)$$

where $\mathbb{M}(m) = \{(n_1, n_2) \in \mathbb{S}^2 \mid n_1 - n_2 = m\}$, i.e., $\mathbb{M}(m)$ is a function that counts the number of sensor pairs with separation m (covariance lag).

IV. PROPOSED DOA ESTIMATION ALGORITHMS

In this section, we present two algorithms for DOA estimation using partially-calibrated arrays. First, we derive the spectrum-based Generalized Coarray Multiple Signal Classification (GCA-MUSIC), followed by its root-version, termed Generalized Coarray Root Multiple Signal Classification (GCA-rMUSIC). Both algorithms rely on the subspace properties of spatial smoothing performed on subcoarrays and on mixing rules for combining the mixed subspaces.

A. Generalized Coarray MUSIC Algorithm

The proposed GCA-MUSIC aims to tackle the case of DoA estimation with partly calibrated sparse subarray geometries. This estimation procedure has many advantages over other techniques presented in the literature: it is capable of exploiting half of the DOF of the subcoarrays, presents super-resolution performance capabilities and has a reasonable trade-off between performance and computational cost. To begin with, we introduce the following definitions:

Definition 8 (Sparse Subarray (SpSub)): The sparse subarrays are each defined as a partially calibrated part of the entire array. Within each sparse subarray, the sensors are coherent; that is, the sampling process is conducted using local oscillators that are synchronized in both frequency and phase, and the relative positions of the sensors within the subarray are known. They are denoted by \mathbb{S}_l , with $l = 1, \dots, L$.

Definition 9 (Subcoarray (SCA)): A subcoarray is defined as the Difference Coarray associated with a given SpSub. They are denoted by \mathbb{D}_l , with $l = 1, \dots, L$.

Definition 10 (Spatially Smoothed Subcoarray (SS-SCA)): A spatially smoothed subcoarray is a SCA with a reduced dimension, which is determined by the parameter choices of a procedure of spatial smoothing. They are denoted by \mathbb{D}_l^i , with $l = 1, \dots, L$ and $i = 1, \dots, M$, where M is both the aperture of each SS-SCA and its quantity.

Notice that each SCA (associated to a specific SpSub), generated according to the mathematical procedure described by (6), (8) and (9), will have a total of M SS-SCA. Then, we have a total of $M \cdot L$ SS-SCA for the whole array.

We consider the SpSub and its respective SCA with central contiguous part (virtual ULA) large enough to allow the recovery of all DOAs of the sources. To simplify the equations, we will assume that the SpSub has a filled SCA (no holes in virtual domain), i.e., the second-order statistics associated to each SpSub contain all the correlation lags from 0 up to $\kappa = (|\mathbb{D}_l| - 1)/2 = (\text{sDoF} - 1)/2$, where sDoF is the number of degrees of freedom for each SCA.

By resorting to the rank properties, it is clear that the outer product $\mathbf{x}_{\mathbb{D}_l} \mathbf{x}_{\mathbb{D}_l}^H$ in (9) is rank deficient. Then, we build up this rank using $M = \kappa + 1 = (\text{sDoF} + 1)/2$ SS-SCA (forward spatial smoothing), for each SCA, according to

$$\mathbf{R}_{\mathbb{D}_l}^{\text{SS}} = \frac{1}{M} \sum_{i=1}^M \mathbf{x}_{\mathbb{D}_l^i} \left(\mathbf{x}_{\mathbb{D}_l^i} \right)^H \quad (17)$$

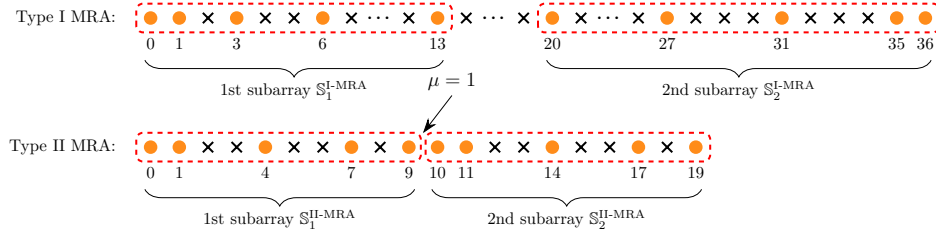


Fig. 1. Type-I and type-II MRA. Notice that the type-II array was generated with a parameter $\mu = 1$ (spacing between subarrays).

where $\mathbf{x}_{\mathbb{D}_l^i} = \mathbf{J}_i \mathbf{x}_{\mathbb{D}_l} \in \mathbb{C}^M$ is the i -th overlapping SS-SCA of the l -th SCA, $\mathbf{J}_i = [\mathbf{0}_{M \times (M-i)}, \mathbf{I}_M, \mathbf{0}_{M \times (i-1)}]$ is a selection matrix, starting ($i = 1$) from the maximum value of the contiguous part of the SCA. Each $\mathbf{R}_{\mathbb{D}_l}^{\text{SS}}$, originated from each of the partially calibrated subarrays provides rough estimates of the sources DoA. The second problem we address is how to integrate the processing to benefit from the estimates of each SpSub in a cohesive manner. This integration of the spectrum is crucial for enhancing estimation performance, as will be demonstrated further.

To perform the signal decomposition, we adopt a similar strategy as described in [5]. The signal and noise subspaces of $\mathbf{R}_{\mathbb{D}_l}^{\text{SS}}$ can be obtained from the following eigenvalue decomposition (EVD):

$$\mathbf{R}_{\mathbb{D}_l}^{\text{SS}} = [\mathbf{U}_l, \mathbf{V}_l] \text{diag}(\beta_1^l, \dots, \beta_M^l) \begin{bmatrix} \mathbf{U}_l^H \\ \mathbf{V}_l^H \end{bmatrix} \quad (18)$$

that has the same eigenvectors as those associated with a covariance matrix whose data were obtained with the first array manifold of the spatial smoothing procedure, denoted by $\mathbf{A}_{\mathbb{D}_l^1}(\boldsymbol{\theta})$ (the virtual array manifold corresponding to the last M rows of $\mathbf{A}_{\mathbb{D}_l}(\boldsymbol{\theta})$). Then, we can state that $\mathcal{R}(\mathbf{A}_{\mathbb{D}_l^1}(\boldsymbol{\theta})) = \mathcal{R}(\mathbf{U}_l)$ and $\mathcal{N}(\mathbf{A}_{\mathbb{D}_l^1}(\boldsymbol{\theta})) = \mathcal{R}(\mathbf{V}_l)$, where $\mathcal{R}(\cdot)$ and $\mathcal{N}(\cdot)$ denote the range and null spaces of a matrix. Particularly in this case, the subarrays are partially-calibrated and so the statistics are divided and must be processed separately up to some degree.

The i -th SS-SCA of the l -th SCA has its signal part contained in $\mathcal{R}(\mathbf{U}_l)$. Define

$$\tilde{\mathbf{U}}_l = \text{blkdiag}(\mathbf{I}_{M(l-1)}, \mathbf{U}_l, \mathbf{I}_{M(L-l)}) \quad (19)$$

and

$$\tilde{\mathbf{V}}_l = \text{blkdiag}(\mathbf{I}_{M(l-1)}, \mathbf{V}_l, \mathbf{I}_{M(L-l)}) \quad (20)$$

Clearly, $\mathcal{R}(\mathbf{U}_l) \subset \mathcal{R}(\tilde{\mathbf{U}}_l)$, i.e., the mixed block-diagonal structure imposes that the range space of $\tilde{\mathbf{U}}_l$ is a superset of the corresponding signal subspace \mathbf{U}_l . However, the signal subspace lies in $\mathcal{R}(\tilde{\mathbf{U}}_l) \forall l \in \{1, \dots, L\}$.

Every affine set is both unbounded and convex. Furthermore, each of the subspaces denoted by $\mathcal{R}(\mathbf{U}_l)$ is affine. Similarly, the corresponding noise subspaces, denoted by $\mathcal{R}(\mathbf{V}_l)$, are also affine. Consider the set

$$\mathbb{W} = \bigcap_{l=1}^L \mathcal{R}(\tilde{\mathbf{V}}_l) \quad (21)$$

In order to project a point onto \mathbb{W} (intersection of noise subspaces), we can iterate through successive projections onto each of the $\mathcal{R}(\tilde{\mathbf{V}}_l)$ by resorting to the method of projection

onto convex sets (POCS) [5], [18], [19]. Since the matrices $\tilde{\mathbf{V}}_l$ are orthogonal, their projection matrices are given by

$$\begin{aligned} \mathbf{P}_{\tilde{\mathbf{V}}_l} &= \tilde{\mathbf{V}}_l \tilde{\mathbf{V}}_l^H \\ &= \text{blkdiag}(\mathbf{I}_{M(l-1)}, \mathbf{V}_l \mathbf{V}_l^H, \mathbf{I}_{M(L-l)}) \end{aligned} \quad (22)$$

The successive projections lead us to

$$\begin{aligned} \mathbf{P} &= \prod_{l=1}^{\tilde{L}} \mathbf{P}_{\tilde{\mathbf{V}}_l} \\ &= \text{blkdiag}(\mathbf{V}_1 \mathbf{V}_1^H, \mathbf{V}_2 \mathbf{V}_2^H, \dots, \mathbf{V}_L \mathbf{V}_L^H) \end{aligned} \quad (23)$$

which is idempotent and thus represents the final matrix after the convergence of POCS. The notation $\prod_{l=1}^{\tilde{L}} \mathbf{A}_l$ means the matrix product $\mathbf{A}_1 \cdot \mathbf{A}_2 \cdot \dots \cdot \mathbf{A}_L$. Let us define the composed steering vector in the SS-SCA coarray domain. We can write

$$\mathbf{a}_{\mathbb{D}}^{\text{SS}}(\boldsymbol{\theta}) = \left[(\mathbf{a}_{\mathbb{D}_1}^{\text{SS}}(\boldsymbol{\theta}))^T, (\mathbf{a}_{\mathbb{D}_2}^{\text{SS}}(\boldsymbol{\theta}))^T, \dots, (\mathbf{a}_{\mathbb{D}_L}^{\text{SS}}(\boldsymbol{\theta}))^T \right]^T \quad (24)$$

where

$$\mathbf{a}_{\mathbb{D}_l}^{\text{SS}}(\boldsymbol{\theta}) = \left[1, e^{j\pi\theta}, \dots, e^{j\pi(M-1)\theta} \right]^T \quad (25)$$

that corresponds to the steering vector of $\mathbf{A}_{\mathbb{D}_l^1}(\boldsymbol{\theta})$ and does not depend on the subarray index l . This comes from the fact that each of the SCA is a filled coarray ULA and has the same number of degrees of freedom $|\mathbb{D}_1| = \dots = |\mathbb{D}_L|$.

The steering vector in (24) is orthogonal to the matrix $\text{blkdiag}(\mathbf{V}_1, \mathbf{V}_2, \dots, \mathbf{V}_L)$. Then, the quadratic form built from the matrix \mathbf{P} and the composite steering vector in (24) should have a null for the true directions $\boldsymbol{\theta}$, similarly to the MUSIC procedure. From that, the pseudo-spectrum can be obtained through

$$\begin{aligned} P(\theta_i^g) &= \frac{1}{(\mathbf{a}_{\mathbb{D}}^{\text{SS}}(\boldsymbol{\theta}_i^g))^H \mathbf{P} (\mathbf{a}_{\mathbb{D}}^{\text{SS}}(\boldsymbol{\theta}_i^g))} \\ &= \frac{1}{\sum_{l=1}^L (\mathbf{a}_{\mathbb{D}_l}^{\text{SS}}(\boldsymbol{\theta}_i^g))^H \mathbf{V}_l \mathbf{V}_l^H \mathbf{a}_{\mathbb{D}_l}^{\text{SS}}(\boldsymbol{\theta}_i^g)}, \quad i \in [g] \end{aligned} \quad (26)$$

where $\boldsymbol{\theta}^g \in (-1, 1]^g$ is a grid, i.e., the discretization of the continuous search area of candidate DOA angles. The true DOAs are estimated as the angles on the grid that maximize (26). GCA-MUSIC is summarized in Algorithm 1.

Remark 2:

- The matrices $\mathbf{R}_{\mathbb{D}_l}^{\text{SS}}$ are orthogonally diagonalizable because of their structure as a sum of outer products (Hermitian symmetric);
- We stress the fact that for SS-SCA with the same number of DoF (virtual aperture) and filled coarray ULAs, the vectors $\mathbf{a}_{\mathbb{D}_l}^{\text{SS}}(\boldsymbol{\theta})$ do not depend on l , as stated in (25).

Algorithm 1: GCA-MUSIC

Input : subarray geometries \mathbb{S}_l , data matrix for each subarray $\hat{\mathbf{X}}_{\mathbb{S}_l}$, grid $\theta^g \in (-1, 1]^g$, number of sources D

```

1 for  $l \leftarrow 1$  to  $L$  do
2    $\hat{\mathbf{R}}_{\mathbb{S}_l} \leftarrow (1/T)\hat{\mathbf{X}}_{\mathbb{S}_l}\hat{\mathbf{X}}_{\mathbb{S}_l}^H$ 
3    $\hat{\mathbf{z}}_{\mathbb{S}_l} \leftarrow \text{vec}(\hat{\mathbf{R}}_{\mathbb{S}_l})$ 
4   Average the repeated elements in  $\mathbf{z}_l$  and sort the
   corresponding coarray locations to obtain  $\hat{\mathbf{x}}_{\mathbb{D}_l}$ 
5    $\hat{\mathbf{R}}_{\mathbb{D}_l}^{\text{SS}} \leftarrow \frac{1}{M} \sum_{i=1}^M \hat{\mathbf{x}}_{\mathbb{D}_l}^i (\hat{\mathbf{x}}_{\mathbb{D}_l}^i)^H$ 
6   Diagonalize  $\hat{\mathbf{R}}_{\mathbb{D}_l}^{\text{SS}}$  through an EVD to find  $\hat{\mathbf{V}}_l$ 
7 for  $i \leftarrow 1$  to  $g$  do
8    $\hat{P}(\theta_i^g) = \left( \sum_{l=1}^L (\mathbf{a}_{\mathbb{D}_l}^{\text{SS}}(\theta_i^g))^H \hat{\mathbf{V}}_l \hat{\mathbf{V}}_l^H \mathbf{a}_{\mathbb{D}_l}^{\text{SS}}(\theta_i^g) \right)^{-1}$ 
9 Find the peaks in  $\hat{P}(\theta_i^g)$  and take the corresponding
   angles as the estimated DOAs

```

Output: Estimated DOAs $\hat{\theta}$

c) The algorithm can indeed be extended for *any* linear sparse subarray geometry, once it has the same physical orientation (not necessarily type-II arrays). Indeed, for algorithms with some SpSub that do not have a filled ULA in the coarray domain, the algorithm can be extended to employ only the central contiguous part of the coarray, i.e., the central part corresponding to the UDoF. In the simulations, an example will illustrate this case.

Lastly, we would like to point out that GCA-MUSIC is capable of identifying more sources than sensors even for the partially calibrated array scenario. GCA-MUSIC can identify up to $(\text{sDoF} - 1)/2$ sources. To write this quantity as a function of the number of physical sensors, we must define the geometry we are dealing with. For example, for sparse subarrays following a NAQ2 geometry, GCA-MUSIC can identify up to $(N/L)^2/2 + N/(2L) - 1$ sources, which is the same number of sources that the coarray MUSIC can identify with a coherent array of N/L sensors with this geometry.

It would be of great interest if we could identify more sources than the number of sensors in the *whole* array. Under certain conditions, GCA-MUSIC can indeed identify more sources than the total number of sensors. For example, for the case of the NAQ2 geometry that we discussed earlier, if we have $L = 3$ subarrays and $N > 16$ in a type-II structure, then the number of sources that can be identified is greater than the number of sensors in the whole arrangement. For example, for $L = 3$ and $N = 18$, GCA-MUSIC allows the identification of up to $D = 20$ sources. This requires a case by case analysis for other geometries.

Additionally, the subarray displacement μ does not have to be known and the subarrays do not need to be collinear. The only requirement is that each SCA has a central contiguous part (\mathbb{U}) that allows the spatial smoothing to be performed on it. In conclusion, it is feasible to use GCA-MUSIC in a heterogeneous subarray scenario incorporating MRA, NAQ2, and other geometrical configurations. Despite the resulting variations in the dimensions of the steering vectors $\mathbf{a}_{\mathbb{D}_l}^{\text{SS}}(\theta)$

and the disparate apertures of each SS-SCA for individual subarrays, the algorithm maintains its capabilities.

B. Generalized coarray root-MUSIC

In order to develop a version of root-MUSIC for partially calibrated sparse arrays, we exploit the root-MUSIC polynomial and the GCA-MUSIC of the previous section. We first review the standard root-MUSIC algorithm in [20].

The steering vector of a coherent ULA can be written as

$$\mathbf{f}(z) = [1, z, z^2, \dots, z^{N-1}]^T \quad (27)$$

which is evaluated at $z = \exp(j\pi\theta)$, assuming an array with N physical sensors. It is widely known that the noise subspace has all their eigenvectors orthogonal to the steering vectors of the array manifold, i.e., $\mathcal{R}(\mathbf{V}) \perp \mathbf{f}(z)$ where \mathbf{V} is a basis for the noise subspace of the coherent ULA and $\mathbf{f}(z) = \mathbf{a}_{\mathbb{S}}(\theta)$ denotes the corresponding array steering vector for the direction θ . The inner product between those two quantities should be zero. From this, we can write the polynomial:

$$\begin{aligned} Q(z) &= \|\mathbf{f}^H(z)\mathbf{V}\|_2^2 \\ &= \mathbf{f}^H(z)\mathbf{V} \left(\mathbf{f}^H(z)\mathbf{V} \right)^H \\ &= (\mathbf{f}^*(z))^T \mathbf{V}\mathbf{V}^H \mathbf{f}(z) \\ &= \mathbf{f}^T(z^*) \mathbf{V}\mathbf{V}^H \mathbf{f}(z) \\ &= \mathbf{f}^T(1/z) \mathbf{V}\mathbf{V}^H \mathbf{f}(z) \end{aligned}$$

which is the polynomial form for the coherent array associated with the projection matrix $\mathbf{V}\mathbf{V}^H$ and the last equality comes from the fact that $|z| = 1$. Notice that in this case, the array geometry must be a ULA. Following the orthogonality conditions, this polynomial must have a zero if evaluated at the true directions. This is the standard root-MUSIC algorithm.

Clearly, in the case of partially calibrated sparse subarrays, where only the second-order statistics of each subarray are available and we do not have access to the cross second-order statistics, a general polynomial must be assembled by resorting to extra tools with the constraint that the subarrays are sparse. As with GCA-MUSIC, here we deal with each of the SpSub after the spatial smoothing procedure as described in (18). In this case, we will use each of the noise subspaces \mathbf{V}_l to obtain a more accurate estimate of the true noise subspace. The proposed procedure relies on the intuition that a more accurate polynomial would be obtained by using the denominator of (26). We assume that each SCA can identify all the sources in the coarray domain.

Inspired by root-MUSIC, we first observe that a vector is in the nullspace of (23) if and only if each of its partitions of appropriate size is in the nullspace of the corresponding block. Consider the partitioned steering vector defined as

$$\mathbf{f}_{\mathbb{D}}(z) = \left[\mathbf{f}_1^T(z), \dots, \mathbf{f}_L^T(z) \right]^T \in \mathbb{C}^{LM_l} \quad (28)$$

where

$$\mathbf{f}_l(z) = [1, z, z^2, \dots, z^{M_l-1}]^T \in \mathbb{C}^{M_l} \quad (29)$$

and $M_l = (\text{sDoF} + 1)/2$. Since each component of (28) is necessarily in the range space of (23), then we can write

$$Q_{\mathbb{D}}(z) = \mathbf{f}_{\mathbb{D}}^T(1/z)\mathbf{P}\mathbf{f}_{\mathbb{D}}(z) = \sum_{l=1}^L \mathbf{f}_l^T(1/z)\mathbf{V}_l\mathbf{V}_l^H\mathbf{f}_l(z) \quad (30)$$

This global coarray polynomial can then be employed to find the true DOAs. Notice that when this substitution is performed, some mathematical implications must be considered. We briefly discuss them in what follows.

We can build this polynomial because each of the SpSub becomes a virtual ULA in the coarray domain. Its degree is a function of the degrees of freedom of the subarrays. The global polynomial in (30) has degree $n_Q = 2M_i - 2$, where $i = \text{argmax}_{l \in \{1, \dots, L\}} M_l$, the index corresponding to the subarray with largest UDoF. Clearly, the higher order coefficients are only affected by the subarrays with large virtual aperture. This observation allows us to further simplify (30) and gain some insight regarding its structure. Based on this polynomial, we can build the global projection matrix as

$$\tilde{\mathbf{P}} = \mathbf{P}_{\mathbf{V}_i} + \sum_{l=1, l \neq i}^L \tilde{\mathbf{P}}_{\mathbf{V}_l} \quad (31)$$

where

$$\tilde{\mathbf{P}}_{\mathbf{V}_l} = \begin{bmatrix} \mathbf{0}_{(M_i - M_l) \times M_l} \\ \mathbf{I}_{M_l} \end{bmatrix} \mathbf{P}_{\mathbf{V}_l} \begin{bmatrix} \mathbf{I}_{M_l} & \mathbf{0}_{M_l \times (M_i - M_l)} \end{bmatrix} \quad (32)$$

Then, we can state that $\tilde{\mathbf{P}}$ is a global noise projection matrix, that accounts for the sum of polynomials and thus represents the noise subspace more accurately compared to the noise subspace of a single subarray. We point out that (31) can even be used in scenarios where the subarrays have different SNRs, by exploiting similar strategies used in antenna diversity techniques [21]. It suffices to apply weights on the noise projections and use an optimization criterion to find the best possible subspace estimate. For the sake of clarity and ease of understanding, we shall confine our analysis to subarrays with the same SNR. By combining (29) and (31), we have

$$Q_{\mathbb{D}}(z) = \mathbf{f}_i^T(1/z)\tilde{\mathbf{P}}\mathbf{f}_i(z), \quad (33)$$

where $i = \text{argmax}_{l \in \{1, \dots, L\}} M_l$, as previously mentioned. After the root pruning process, only the D roots inside and closest to the unit circle are considered.

We highlight that GCA-rMUSIC is capable of estimating more sources than the number of sensors in each subarray, as it significantly increases the polynomial degree. Moreover, while root-MUSIC requires the array to be fully synchronized, GCA-rMUSIC, summarized in Algorithm 2, can estimate directions based on a global estimate of the nullspace.

V. ANALYSIS

In this section, we present an analysis of degrees of freedom of the proposed subarray geometries, an assessment of the computational cost of the proposed DOA estimation algorithms, an evaluation of their identifiability properties and derive a CRLB.

Algorithm 2: GCA-rMUSIC

Input : subarray geometries \mathbb{S}_l , data matrix for each subarray $\hat{\mathbf{X}}_{\mathbb{S}_l}$, grid $\theta^g \in (-1, 1]^g$, number of sources D

- 1 **for** $l \leftarrow 1$ **to** L **do**
- 2 $\hat{\mathbf{R}}_{\mathbb{S}_l} \leftarrow (1/T)\hat{\mathbf{X}}_{\mathbb{S}_l}\hat{\mathbf{X}}_{\mathbb{S}_l}^H$
- 3 $\mathbf{z}_l \leftarrow \text{vec}(\hat{\mathbf{R}}_{\mathbb{S}_l})$
- 4 Average the repeated elements in \mathbf{z}_l and sort the corresponding coarray locations to obtain $\mathbf{x}_{\mathbb{D}_l}$
- 5 $\mathbf{R}_{\mathbb{D}_l}^{SS} \leftarrow \frac{1}{M} \sum_{i=1}^M \mathbf{x}_{\mathbb{D}_l}^i (\mathbf{x}_{\mathbb{D}_l}^i)^H$
- 6 Diagonalize $\mathbf{R}_{\mathbb{D}_l}^{SS}$ through an EVD to find \mathbf{V}_l
- 7 $\mathbf{P}_{\mathbf{V}_l} \leftarrow \mathbf{V}_l\mathbf{V}_l^H$
- 8 Search for $i = \text{argmax}_{l \in \{1, \dots, L\}} M_l$
- 9 $\tilde{\mathbf{P}} = \mathbf{P}_{\mathbf{V}_i} + \sum_{l=1, l \neq i}^L \tilde{\mathbf{P}}_{\mathbf{V}_l}$
- 10 Find the roots of $Q_{\mathbb{D}}(z) = \mathbf{f}_i^T(1/z)\tilde{\mathbf{P}}\mathbf{f}_i(z)$
- 11 Select the D roots inside and closest to the unit circle as \hat{z}_d
- 12 Estimate the DOAs according to $\hat{\theta} = (\angle \hat{z}_d) / \pi$

Output: Estimated DOAs $\hat{\theta}$

A. Analysis of degrees of freedom

A natural question that arises from the above introduced (sub)array geometries is related to the manifold structure, as well as the DoF for a difference coarray scenario [4], [22]. In this section, we shed light upon these two important aspects.

1) *Type-I*: clearly, for type-I arrays there is no *a priori* analytical relation between the subarray manifolds, due to the fact that the geometries change dramatically between subarrays. Also, the number of DoF for the predefined geometry and its type-I counterpart is obviously the same, for the case in which we keep the original intersubarray displacement and both geometries coincide. Moreover, there is no general rule to predict the DoF associated to the subarrays. This requires an analysis case by case for the sparse geometry employed.

2) *Type-II*: some analytical relations can be straightforwardly derived. In this case, to simplify the equations, we will assume that the subarrays are multiple invariant, i.e., they attend the sufficient condition of having the same number of physical sensors N/L and thus the same aperture. Using the array manifold of the whole array expressed in matrix form, we can write

$$\mathbf{A}_{\mathbb{S}} = [\mathbf{A}_{\mathbb{S}_1}^T, (\mathbf{A}_{\mathbb{S}_1} \mathbf{\Lambda}^{\Delta})^T, \dots, (\mathbf{A}_{\mathbb{S}_1} \mathbf{\Lambda}^{(L-1)\Delta})^T]^T \quad (34)$$

where we dropped the dependence of the manifold on the DOAs to simplify the notation. The matrix $\mathbf{\Lambda}$ is defined as

$$\mathbf{\Lambda} = \text{diag}(e^{j\pi\theta_1}, \dots, e^{j\pi\theta_D}) \quad (35)$$

The multiple exponents of $\mathbf{\Lambda}$ in (34) represent the subarray translations along the straight line and are assumed to be $\Delta = \mu + \kappa$ (see Definition 2).

In what follows, we establish our most important result [14]: the number of DoF for type-II arrays is upper-bounded by a function of the DoF of the subarrays (sDoF), which can be theoretically calculated for a variety of geometries. This result is quantitatively described in Theorem 1.

Theorem 1: Consider a type-II array with geometry as defined in Definition 2 with equal-aperture subarrays. If $1 \leq \mu \leq \kappa$, then the number of DoF of the array \mathbb{S} is upper-bounded by $L(\text{sDoF} - 1) + 2(L - 1)\mu + 1$, where sDoF is the number of DoF for each subarray. If $\mu > \kappa$, then the number of DoF is equal to $(2L - 1)\text{sDoF}$.

Proof: Let $c(n)$ be a discrete-valued function that assumes the value of 1 if there is a sensor at n or 0 otherwise. This function for a type-II array is given by $c(n) = c_1(n) + \dots + c_L(n)$. Since the subarrays are translated versions of the reference array, $c_l(n) = c_1(n - \Delta_l)$, where $\Delta_l = (l - 1)\Delta$. The weight function associated to that array (counts the number of spatial correlations with lag n) is defined through [2] $w(n) = c(n) \otimes c^-(n)$, where $c^-(n)$ is the time reversal version of $c(n)$ and \otimes denotes the digital convolution between two sequences. Then, one can write

$$\begin{aligned} w(n) &= \left(\sum_{i=1}^L c_i(n) \right) \otimes \left(\sum_{j=1}^L c_j^-(n) \right) \\ &= \sum_{i,j=1}^L c_1(n - (i - 1)\Delta) \otimes c_1^-(n - (j - 1)\Delta) \\ &= \sum_{i,j=1}^L c_1(n) \otimes c_1^-(n) \otimes \delta(n - \Delta_i + \Delta_j) \\ &= \sum_{i,j=1}^L w_1(n - \Delta_i + \Delta_j) \end{aligned} \quad (36)$$

The number of DoF is the cardinality of the support of $w(n)$. This support set has always an odd number of elements, given that $w(n)$ is an even function. Clearly, from (36), the weight function of the reference array $w_1(n)$ is repeated along the domain with displacement factors given by $\Delta_j - \Delta_i$. Since $|\text{supp}(w_1(n))| = \text{sDoF}$ and for $\mu > \kappa$ there is no superposition of the weight functions of the subarrays with a different $\Delta_j - \Delta_i$, then $|\text{supp}(w(n))| = (2L - 1)|\text{supp}(w_1(n))| \Rightarrow \text{DoF} = (2L - 1)\text{sDoF}$. Note that there are $2L - 1$ diagonals in a $L \times L$ matrix representing all possible $\Delta_j - \Delta_i$. For $1 \leq \mu \leq \kappa$, the superposition implies that the support set of $w(n)$ ranges from $-(L - 1)\Delta - \kappa$ to $(L - 1)\Delta + \kappa$. Since $\kappa = (\text{sDoF} - 1)/2$, the support set of $w(n)$ has a maximum number of elements equal to $2[(L - 1)\Delta + \kappa] + 1$ or $L(\text{sDoF} - 1) + 2(L - 1)\mu + 1$. The equality holds if the difference coarray of the subarrays has no holes (no missing lags), as it indeed happens for many geometries like NAQ2 and (restricted) MRAs. ■

B. Arithmetic complexity

In terms of computational complexity, we can count the number of arithmetic operations such as additions and multiplications for each algorithm as it is described in what follows. For GCA-MUSIC, we have:

- a) **Step S1: estimation of covariance matrix.** This step computes each of the subarrays' received signal covariance matrix by means of its sample covariance estimate. Since the outer products involve vectors of dimension $N_l = N/L$, then the number of required additions and multiplications is $L[(T - 1)(N/L)^2]$ and $L[T(N/L)^2]$, respectively.⁴

⁴Notice that we consider the case where all the subarrays have the same number of physical sensors to simplify the final expressions.

TABLE I
ARITHMETIC COMPLEXITY ANALYSIS OF GCA-MUSIC

step	type of operation	
	additions	multiplications
S1	$L(T - 1)(N/L)^2$	$LT(N/L)^2$
S2	$L(T - 1)M^2$	$LT M^2$
S3	$4M^3/3 + \mathcal{O}(M^2)$	
S4	$L(B - 1)M^2$	LBM^2
S5	$g(LBM^2 - L)$	$g(L(B + 1)M^2 + LM)$
TOTAL	$4M^3/3 + \mathcal{O}(M^2)$	

- b) **Step S2: estimation of spatially-smoothed coarray covariance matrix.** In this case, the coarrays outer products are obtained from vectors of dimension M (see (17)). Then, the number of additions and multiplications is $L \cdot [(T - 1)M^2]$ and $L \cdot [TM^2]$, respectively;
- c) **Step S3: EVD of $\mathbf{R}_{\mathbb{D}_l}^{\text{SS}}$.** Since the decompositions involve a square matrix of dimension M , the EVD takes about $4M^3/3 + \mathcal{O}(M^2)$ operations;
- d) **Step S4: noise subspace projection matrices.** The projection matrix $\mathbf{P}_{\mathbf{V}_l} = \mathbf{V}_l \mathbf{V}_l^H = \mathbf{I} - \mathbf{U}_l \mathbf{U}_l^H$ requires $L \cdot (B - 1)M^2$ additions and LBM^2 multiplications, as it involves L matrices of size $M \times B$, where $B = M - D$;
- e) **Step S5: pseudo-spectrum calculation.** The pseudo-spectrum, for each point in the grid, is calculated through $(\mathbf{a}_{\mathbb{D}_l}^{\text{SS}}(\theta_i^g))^H \hat{\mathbf{V}}_l \hat{\mathbf{V}}_l^H \mathbf{a}_{\mathbb{D}_l}^{\text{SS}}(\theta_i^g)$. It involves $LBM^2 - L$ additions and $L(B + 1)M^2 + LM$ multiplications for each of the points in the grid. For a grid search with g points the complexity for the whole search is $g(LBM^2 - L)$ additions and $g(L(B + 1)M^2 + LM)$ multiplications.

The arithmetic complexity is summarized in Table I.

For GCA-rMUSIC, the steps S1-S4 are the same as those of GCA-MUSIC. For conciseness, we do not repeat them here. The additional steps are described in what follows.

- a) **Step S5: averaged projection matrix calculation.** The averaged projection matrix is calculated by (27) and involves $(LB - 1)M^2$ additions and $(LB + 1)M^2$ multiplications.
- b) **Step S6: polynomial root-finding.** This technique relies on the SVD of a square matrix (companion matrix) whose dimension coincides with the polynomial degree [23]. Then, since the coarray polynomial in (30) has degree $2M - 2$, this step takes about $32M^3/3 + \mathcal{O}(M^2)$ operations.

C. Identifiability

According to the analysis proposed in [13], which establishes the identifiability conditions for non-coherent processing schemes, we can further investigate the properties of type-II arrays regarding identifiability. For that, we assume that the subarrays have an arbitrary number of sensors. The composed coarray manifold for type-II arrays is given by

$$\mathbf{A}_{\mathbb{D}} = \left[\mathbf{A}_{\mathbb{D}_1}^T, \dots, \mathbf{A}_{\mathbb{D}_L}^T \right]^T \quad (37)$$

The maximum number of identifiable sources is given by the sufficient condition $D \leq \lfloor \rho/2 \rfloor$, where ρ is the Kruskal rank of (37). Let us analyze two main cases separately: subarrays with the same and a different number of sensors. For subarrays with the same number of sensors, $\rho_{\mathbf{A}_{\mathbb{D}}} = \rho_{\mathbf{A}_{\mathbb{D}_l}}$ and thus the SCA length determines the maximum number of identifiable sources. In this particular case, $M - 1$. On the other hand,

if the subarrays have a different number of sensors, then the identifiability will be limited by the subarray with the largest aperture. In this case, $D \leq \lfloor \max_l(\rho_{\mathbf{A}_{D_l}})/2 \rfloor$.

D. Derivation of the CRLB for the partially-calibrated scheme

In this section, we derive a CRLB for partially-calibrated arrays. Unlike the approach presented in [13], our proposed CRLB assumes that the impinging source signals are spatially coherent across all subarrays. Additionally, the bound outlined in [7] is not applicable under two specific conditions: 1) when the number of sources exceeds the total number of sensors across all subarrays, and 2) when the sources are assumed to be uncorrelated *a priori*. Our proposed bound overcomes these limitations.

In order to derive the CRLB, we define the parameter vector as

$$\phi = \left[\boldsymbol{\theta}^T, \mathbf{p}^T, \sigma_n^2, \boldsymbol{\nu}_2^T, \dots, \boldsymbol{\nu}_L^T, \boldsymbol{\eta}_2^T, \dots, \boldsymbol{\eta}_L^T \right] \quad (38)$$

where

$$\begin{aligned} \boldsymbol{\nu}_l &= \Re \left\{ [\mathbf{h}_{l,1}, \dots, \mathbf{h}_{l,D}]^T \right\} \\ \boldsymbol{\eta}_l &= \Im \left\{ [\mathbf{h}_{l,1}, \dots, \mathbf{h}_{l,D}]^T \right\} \end{aligned} \quad (39)$$

Let us find the Fisher Information Matrix (FIM) associated with the estimation of the vector ϕ , that is defined as

$$\text{FIM} = -E \left\{ \frac{\partial^2 \ln p(\mathbf{x}_{\mathbb{S}}(t); \phi)}{\partial \phi_i \partial \phi_j} \right\}, \quad (40)$$

where $p(\mathbf{x}_{\mathbb{S}}(t); \phi)$ is the probability density function of $\mathbf{x}_{\mathbb{S}}(t)$ which depends on the nonrandom parameter vector ϕ . The covariance matrix of the data model is such that $x_{\mathbb{S}}(t) \sim \mathcal{CN}(0, \mathbf{R}_{\mathbb{S}})$ and

$$\mathbf{R}_{\mathbb{S}} = \tilde{\mathbf{V}}(\boldsymbol{\theta}) \tilde{\mathbf{H}} \mathbf{R}_s \tilde{\mathbf{H}}^H \tilde{\mathbf{V}}^H(\boldsymbol{\theta}) + \sigma_n^2 \mathbf{I} \quad (41)$$

The log-likelihood for a single snapshot is given by [1]

$$\mathcal{L}_{\mathbf{x}}(\phi) = -\ln |\pi \mathbf{R}_{\mathbb{S}}(\phi)| - \mathbf{x}^H \mathbf{R}_{\mathbb{S}}^{-1}(\phi) \mathbf{x} \quad (42)$$

The elements of the FIM are given by

$$\begin{aligned} [\text{FIM}]_{ij} &= -E \left[\frac{\partial^2 \mathcal{L}_{\mathbf{x}}(\phi)}{\partial \phi_i \partial \phi_j} \right] \\ &= T \text{tr} \left[\mathbf{R}_{\mathbb{S}}^{-1}(\phi) \frac{\partial \mathbf{R}_{\mathbb{S}}(\phi)}{\partial \phi_i} \mathbf{R}_{\mathbb{S}}^{-1}(\phi) \frac{\partial \mathbf{R}_{\mathbb{S}}(\phi)}{\partial \phi_j} \right] \end{aligned} \quad (43)$$

Before we calculate the derivatives in (43), we first divide the parameter vector into two blocks, as follows

$$\phi = [\phi_1^T \quad \phi_2^T]^T \quad (44)$$

where $\phi_1 = \boldsymbol{\theta}$ and $\phi_2 = [\mathbf{p}^T, \sigma_n^2, \boldsymbol{\nu}_2^T, \dots, \boldsymbol{\nu}_L^T, \boldsymbol{\eta}_2^T, \dots, \boldsymbol{\eta}_L^T]^T$. The FIM matrix can be partitioned as

$$\text{FIM} = \begin{bmatrix} \text{FIM}_{\phi_1 \phi_1} & \text{FIM}_{\phi_1 \phi_2} \\ \text{FIM}_{\phi_2 \phi_1} & \text{FIM}_{\phi_2 \phi_2} \end{bmatrix} \quad (45)$$

The CRLB matrix is defined as

$$\mathbf{C}_{\text{CRLB}}(\phi) = \begin{bmatrix} \mathbf{C}_{\text{CRLB}}(\phi_1 \phi_1) & \mathbf{C}_{\text{CRLB}}(\phi_1 \phi_2) \\ \mathbf{C}_{\text{CRLB}}(\phi_2 \phi_1) & \mathbf{C}_{\text{CRLB}}(\phi_2 \phi_2) \end{bmatrix} \quad (46)$$

Due to the fact that $\mathbf{C}_{\text{CRLB}}(\phi) = \text{FIM}^{-1}$ and using the inverse formula for a block-partitioned matrix, we have

$$\mathbf{C}_{\text{CRLB}}(\phi_1 \phi_1) = \left[\text{FIM}_{\phi_1 \phi_1} - \text{FIM}_{\phi_1 \phi_2} \times \text{FIM}_{\phi_2 \phi_2}^{-1} \text{FIM}_{\phi_2 \phi_1} \right]^{-1} \quad (47)$$

Since we are mainly interested in the estimation of the direction parameters, we are seeking the matrix $\mathbf{C}_{\text{CRLB}}(\phi_1 \phi_1)$. Let us proceed with the computation of each of the FIM blocks in (47) using the expression in (43) with the corresponding partial derivatives.

In order to do so, we calculate the FIM matrices related to the variables in the parameter vector ϕ , as well as their crossed FIMs. The key in the derivation process is to:

- Compute the derivatives $\partial \mathbf{R}_{\mathbb{S}}(\phi) / \partial \phi_i$;
- Put the resulting expression in (43) in a compact form. We proceed as follows:

I) Computation of derivatives

- Derivative with respect to $\boldsymbol{\theta}$:

$$\begin{aligned} \frac{\partial \mathbf{R}_{\mathbb{S}}(\phi)}{\partial \theta_i} &= \frac{\partial \tilde{\mathbf{V}}(\boldsymbol{\theta}) \tilde{\mathbf{H}}}{\partial \theta_i} \mathbf{R}_s \tilde{\mathbf{H}}^H \tilde{\mathbf{V}}^H(\boldsymbol{\theta}) \\ &\quad + \tilde{\mathbf{V}}(\boldsymbol{\theta}) \tilde{\mathbf{H}} \mathbf{R}_s \frac{\partial \tilde{\mathbf{H}}^H \tilde{\mathbf{V}}^H(\boldsymbol{\theta})}{\partial \theta_i} \end{aligned} \quad (48)$$

The derivatives $\partial(\tilde{\mathbf{V}}(\boldsymbol{\theta}) \tilde{\mathbf{H}}) / \partial \theta_i$ can be represented in compact form as

$$\frac{\partial \tilde{\mathbf{V}}(\boldsymbol{\theta}) \tilde{\mathbf{H}}}{\partial \theta_i} = \mathbf{D} \mathbf{e}_i \mathbf{e}_i^T \quad (49)$$

where

$$\mathbf{D} = \left[\frac{\partial \mathbf{V}(\boldsymbol{\theta}_1) \mathbf{h}_1}{\partial \theta_1}, \dots, \frac{\partial \mathbf{V}(\boldsymbol{\theta}_D) \mathbf{h}_D}{\partial \theta_D} \right] \quad (50)$$

for which \mathbf{e}_i corresponds to the i -th canonical basis vector with all zeros except for a 1 in the i -th position. The goal of the outer product (projection) of the canonical basis vectors is to isolate the i -th column of \mathbf{D} and simultaneously nullify all its other columns. Notice that the parameters $\tilde{\mathbf{H}}$ are a function of the DOA sources in the general case.

By substituting (49) in (48), we have:

$$\frac{\partial \mathbf{R}_{\mathbb{S}}(\phi)}{\partial \theta_i} = \mathbf{D} \mathbf{e}_i \mathbf{e}_i^T \mathbf{R}_s \mathbf{W}^H + \mathbf{W} \mathbf{R}_s \mathbf{e}_i \mathbf{e}_i^T \mathbf{D}^H \quad (51)$$

where

$$\begin{aligned} \mathbf{W} &\triangleq \tilde{\mathbf{V}}(\boldsymbol{\theta}) \tilde{\mathbf{H}} \\ &= [\mathbf{V}(\boldsymbol{\theta}_1) \mathbf{h}_1, \dots, \mathbf{V}(\boldsymbol{\theta}_D) \mathbf{h}_D] \end{aligned} \quad (52)$$

$$\mathbf{R}_s = \text{diag}(\mathbf{p}) \quad (53)$$

- Derivative with respect to \mathbf{p} (source powers)

$$\begin{aligned} \frac{\partial \mathbf{R}_{\mathbb{S}}(\phi)}{\partial p_i} &= \mathbf{W} \frac{\partial \mathbf{R}_s}{\partial p_i} \mathbf{W}^H \\ &= \mathbf{w}_i \mathbf{w}_i^H \end{aligned} \quad (54)$$

where \mathbf{w}_i is the i -th column of \mathbf{W} , defined in (52).

- Derivative with respect to σ_n^2

From (41) the derivative of the covariance matrix with respect to the noise variance is given by

$$\frac{\partial \mathbf{R}_S(\phi)}{\partial \sigma_n^2} = \mathbf{I} \quad (55)$$

- Derivatives with respect to the real part of the calibration parameters ν_l

$$\frac{\partial \mathbf{R}_S(\phi)}{\partial \nu_{l,i}} = \frac{\partial \mathbf{W}}{\partial \nu_{l,i}} \mathbf{R}_s \mathbf{W}^H + \mathbf{W} \mathbf{R}_s \frac{\partial \mathbf{W}^H}{\partial \nu_{l,i}} \quad (56)$$

The derivatives $\partial \mathbf{W} / \partial \nu_{l,i}$ can be represented as

$$\frac{\partial \mathbf{W}}{\partial \nu_{l,i}} = \mathbf{P}_{\mathbf{E}_l} \mathbf{A} \mathbf{e}_i \mathbf{e}_i^T \quad (57)$$

where

$$\begin{aligned} \mathbf{P}_{\mathbf{E}_l} &= \mathbf{E}_l \mathbf{E}_l^T, \quad \mathbf{E}_l = [\mathbf{0}_{a_l \times N_l}^T \quad \mathbf{I}_{N_l \times N_l} \quad \mathbf{0}_{b_l \times N_l}^T]^T \\ a_l &= \sum_{i=1}^{l-1} N_i, \quad b_l = \sum_{i=l+1}^L N_i \\ \mathbf{A} &= [\mathbf{A}_{S_1}^T(\boldsymbol{\theta}), \dots, \mathbf{A}_{S_L}^T(\boldsymbol{\theta})]^T \end{aligned} \quad (58)$$

By substituting (57) in (56), we can write

$$\frac{\partial \mathbf{R}_S(\phi)}{\partial \nu_{l,i}} = \mathbf{P}_{\mathbf{E}_l} \mathbf{A} \mathbf{e}_i \mathbf{e}_i^T \mathbf{R}_s \mathbf{W}^H + \mathbf{W} \mathbf{R}_s \mathbf{e}_i \mathbf{e}_i^T \mathbf{A}^H \mathbf{P}_{\mathbf{E}_l} \quad (59)$$

- Derivatives with respect to the imaginary part of the calibration parameters η_l

Due to the structure and relation between ν_l and η_l , the derivatives $\partial \mathbf{W} / \partial \eta_{l,i}$ follow immediately from (57) as

$$\begin{aligned} \frac{\partial \mathbf{W}}{\partial \eta_{l,i}} &= j \frac{\partial \mathbf{W}}{\partial \nu_{l,i}} \\ &= j \mathbf{P}_{\mathbf{E}_l} \mathbf{A} \mathbf{e}_i \mathbf{e}_i^T \end{aligned} \quad (60)$$

The derivative of the covariance matrix with respect to $\eta_{l,i}$ is given by

$$\frac{\partial \mathbf{R}_S(\phi)}{\partial \eta_{l,i}} = \frac{\partial \mathbf{W}}{\partial \eta_{l,i}} \mathbf{R}_s \mathbf{W}^H + \mathbf{W} \mathbf{R}_s \frac{\partial \mathbf{W}^H}{\partial \eta_{l,i}} \quad (61)$$

By replacing (60) into (61) results in

$$\begin{aligned} \frac{\partial \mathbf{R}_S(\phi)}{\partial \eta_{l,i}} &= j \left(\mathbf{P}_{\mathbf{E}_l} \mathbf{A} \mathbf{e}_i \mathbf{e}_i^T \mathbf{R}_s \mathbf{W}^H - \right. \\ &\quad \left. \mathbf{W} \mathbf{R}_s \mathbf{e}_i \mathbf{e}_i^T \mathbf{A}^H \mathbf{P}_{\mathbf{E}_l} \right) \end{aligned} \quad (62)$$

II) Calculation of the FIM matrices

- FIM matrix with respect to the DOAs $\boldsymbol{\theta}$

By substituting (51) into (43), we have

$$\begin{aligned} [\text{FIM}_{\boldsymbol{\theta}\boldsymbol{\theta}}]_{ij} &= \\ T \text{tr} \{ &\mathbf{R}_S^{-1} \mathbf{D} \mathbf{e}_i \mathbf{e}_i^T \mathbf{R}_s \mathbf{W}^H \mathbf{R}_S^{-1} \mathbf{D} \mathbf{e}_j \mathbf{e}_j^T \mathbf{R}_s \mathbf{W}^H \\ &+ \mathbf{R}_S^{-1} \mathbf{D} \mathbf{e}_i \mathbf{e}_i^T \mathbf{R}_s \mathbf{W}^H \mathbf{R}_S^{-1} \mathbf{W} \mathbf{R}_s \mathbf{e}_j \mathbf{e}_j^T \mathbf{D}^H \\ &+ \mathbf{R}_S^{-1} \mathbf{W} \mathbf{R}_s \mathbf{e}_i \mathbf{e}_i^T \mathbf{D}^H \mathbf{R}_S^{-1} \mathbf{D} \mathbf{e}_j \mathbf{e}_j^T \mathbf{R}_s \mathbf{W}^H \\ &+ \mathbf{R}_S^{-1} \mathbf{W} \mathbf{R}_s \mathbf{e}_i \mathbf{e}_i^T \mathbf{D}^H \mathbf{R}_S^{-1} \mathbf{W} \mathbf{R}_s \mathbf{e}_j \mathbf{e}_j^T \mathbf{D}^H \} \end{aligned} \quad (63)$$

By applying the cyclic property of the trace, we obtain:

$$\begin{aligned} [\text{FIM}_{\boldsymbol{\theta}\boldsymbol{\theta}}]_{ij} &= \\ T \text{tr} \{ &(\mathbf{e}_j^T \mathbf{R}_s \mathbf{W}^H \mathbf{R}_S^{-1} \mathbf{D} \mathbf{e}_i)(\mathbf{e}_i^T \mathbf{R}_s \mathbf{W}^H \mathbf{R}_S^{-1} \mathbf{D} \mathbf{e}_j) \\ &+ (\mathbf{e}_j^T \mathbf{R}_s \mathbf{W}^H \mathbf{R}_S^{-1} \mathbf{W} \mathbf{R}_s \mathbf{e}_i)(\mathbf{e}_i^T \mathbf{D}^H \mathbf{R}_S^{-1} \mathbf{D} \mathbf{e}_j) \\ &+ (\mathbf{e}_j^T \mathbf{D}^H \mathbf{R}_S^{-1} \mathbf{D} \mathbf{e}_i)(\mathbf{e}_i^T \mathbf{R}_s \mathbf{W}^H \mathbf{R}_S^{-1} \mathbf{W} \mathbf{R}_s \mathbf{e}_j) \\ &+ (\mathbf{e}_j^T \mathbf{D}^H \mathbf{R}_S^{-1} \mathbf{W} \mathbf{R}_s \mathbf{e}_i)(\mathbf{e}_i^T \mathbf{D}^H \mathbf{R}_S^{-1} \mathbf{W} \mathbf{R}_s \mathbf{e}_j) \} \end{aligned} \quad (64)$$

which can be rewritten without the trace as:

$$\begin{aligned} [\text{FIM}_{\boldsymbol{\theta}\boldsymbol{\theta}}]_{ij} &= \\ 2T \Re \{ &(\mathbf{e}_i^T \mathbf{R}_s \mathbf{W}^H \mathbf{R}_S^{-1} \mathbf{D} \mathbf{e}_j)(\mathbf{e}_j^T \mathbf{R}_s \mathbf{W}^H \mathbf{R}_S^{-1} \mathbf{D} \mathbf{e}_i) \\ &+ (\mathbf{e}_i^T \mathbf{R}_s \mathbf{W}^H \mathbf{R}_S^{-1} \mathbf{W} \mathbf{R}_s \mathbf{e}_j)(\mathbf{e}_j^T \mathbf{D}^H \mathbf{R}_S^{-1} \mathbf{D} \mathbf{e}_i) \} \end{aligned} \quad (65)$$

or in matrix form

$$\begin{aligned} \text{FIM}_{\boldsymbol{\theta}\boldsymbol{\theta}} &= \\ 2T \Re \{ &(\mathbf{R}_s \mathbf{W}^H \mathbf{R}_S^{-1} \mathbf{D}) \odot (\mathbf{R}_s \mathbf{W}^H \mathbf{R}_S^{-1} \mathbf{D})^T \\ &+ (\mathbf{R}_s \mathbf{W}^H \mathbf{R}_S^{-1} \mathbf{W} \mathbf{R}_s) \odot (\mathbf{D}^H \mathbf{R}_S^{-1} \mathbf{D})^T \} \end{aligned} \quad (66)$$

where \odot denotes the Hadamard product. Due to space constraints, only the final results of the subsequently computed FIMs are presented.

- FIM matrix with respect to the sources powers \mathbf{p}

By replacing (54) into (43), we can write

$$\text{FIM}_{\mathbf{p}\mathbf{p}} = T(\mathbf{W}^H \mathbf{R}_S^{-1} \mathbf{W}) \odot (\mathbf{W}^H \mathbf{R}_S^{-1} \mathbf{W})^T \quad (67)$$

- FIM matrix with respect to the noise power σ_n^2

By substituting (55) into (43), we arrive at

$$\text{FIM}_{\sigma_n^2 \sigma_n^2} = T \text{tr} [\mathbf{R}_S^{-2}] \quad (68)$$

- FIM matrix with respect to the real part of the calibration parameters ν_l

By substituting (59) into (43), we can write

$$\begin{aligned} \text{FIM}_{\nu_l \nu_k} &= \\ 2T \Re \{ &(\mathbf{R}_s \mathbf{W}^H \mathbf{R}_S^{-1} \mathbf{P}_{\mathbf{E}_k} \mathbf{A}) \odot (\mathbf{R}_s \mathbf{W}^H \mathbf{R}_S^{-1} \mathbf{P}_{\mathbf{E}_l} \mathbf{A})^T \\ &+ (\mathbf{R}_s \mathbf{W}^H \mathbf{R}_S^{-1} \mathbf{W} \mathbf{R}_s) \odot (\mathbf{A}^H \mathbf{P}_{\mathbf{E}_k} \mathbf{R}_S^{-1} \mathbf{P}_{\mathbf{E}_l} \mathbf{A})^T \} \end{aligned} \quad (69)$$

- FIM matrix with respect to the imaginary part of the calibration parameters η_l

By substituting (62) into (43), we can write

$$\begin{aligned} \text{FIM}_{\eta_l \eta_k} &= \\ -2T \Re \{ &(\mathbf{R}_s \mathbf{W}^H \mathbf{R}_S^{-1} \mathbf{P}_{\mathbf{E}_k} \mathbf{A}) \odot (\mathbf{R}_s \mathbf{W}^H \mathbf{R}_S^{-1} \mathbf{P}_{\mathbf{E}_l} \mathbf{A})^T \\ &- (\mathbf{R}_s \mathbf{W}^H \mathbf{R}_S^{-1} \mathbf{W} \mathbf{R}_s) \odot (\mathbf{A}^H \mathbf{P}_{\mathbf{E}_k} \mathbf{R}_S^{-1} \mathbf{P}_{\mathbf{E}_l} \mathbf{A})^T \} \end{aligned} \quad (70)$$

- FIM matrix with respect to $\boldsymbol{\theta}$ and \mathbf{p}

$$\text{FIM}_{\boldsymbol{\theta}\mathbf{p}} = 2T \Re \{ (\mathbf{R}_s \mathbf{W}^H \mathbf{R}_S^{-1} \mathbf{W}) \odot (\mathbf{W}^H \mathbf{R}_S^{-1} \mathbf{D})^T \} \quad (71)$$

- FIM matrix with respect to $\boldsymbol{\theta}$ and σ_n^2

$$\text{FIM}_{\boldsymbol{\theta}\sigma_n^2} = 2T \text{diag}^M (\Re \{ \mathbf{R}_s \mathbf{W}^H \mathbf{R}_S^{-2} \mathbf{D} \}) \quad (72)$$

where $\text{diag}^M(\mathbf{X})$ is a column vector whose elements consists of the diagonal elements of square-matrix \mathbf{X} .

h) FIM matrix with respect to θ and ν_l

$$\begin{aligned} \text{FIM}_{\theta\nu_l} &= \\ &= T\{(\mathbf{R}_s \mathbf{W}^H \mathbf{R}_s^{-1} \mathbf{P}_{\mathbf{E}_l} \mathbf{A}) \odot (\mathbf{R}_s \mathbf{W}^H \mathbf{R}_s^{-1} \mathbf{D})^T \\ &+ (\mathbf{R}_s \mathbf{W}^H \mathbf{R}_s^{-1} \mathbf{W} \mathbf{R}_s) \odot (\mathbf{A}^H \mathbf{P}_{\mathbf{E}_l} \mathbf{R}_s^{-1} \mathbf{D})^T \\ &+ (\mathbf{D}^H \mathbf{R}_s^{-1} \mathbf{P}_{\mathbf{E}_l} \mathbf{A}) \odot (\mathbf{R}_s \mathbf{W}^H \mathbf{R}_s^{-1} \mathbf{W} \mathbf{R}_s)^T \\ &+ (\mathbf{D}^H \mathbf{R}_s^{-1} \mathbf{W} \mathbf{R}_s) \odot (\mathbf{A}^H \mathbf{P}_{\mathbf{E}_l} \mathbf{R}_s^{-1} \mathbf{W} \mathbf{R}_s)^T\} \end{aligned} \quad (73)$$

i) FIM matrix with respect to θ and η_l

$$\begin{aligned} \text{FIM}_{\theta\eta_l} &= \\ &= jT\{(\mathbf{R}_s \mathbf{W}^H \mathbf{R}_s^{-1} \mathbf{P}_{\mathbf{E}_l} \mathbf{A}) \odot (\mathbf{R}_s \mathbf{W}^H \mathbf{R}_s^{-1} \mathbf{D})^T \\ &- (\mathbf{R}_s \mathbf{W}^H \mathbf{R}_s^{-1} \mathbf{W} \mathbf{R}_s) \odot (\mathbf{A}^H \mathbf{P}_{\mathbf{E}_l} \mathbf{R}_s^{-1} \mathbf{D})^T \\ &+ (\mathbf{D}^H \mathbf{R}_s^{-1} \mathbf{P}_{\mathbf{E}_l} \mathbf{A}) \odot (\mathbf{R}_s \mathbf{W}^H \mathbf{R}_s^{-1} \mathbf{W} \mathbf{R}_s)^T \\ &- (\mathbf{D}^H \mathbf{R}_s^{-1} \mathbf{W} \mathbf{R}_s) \odot (\mathbf{A}^H \mathbf{P}_{\mathbf{E}_l} \mathbf{R}_s^{-1} \mathbf{W} \mathbf{R}_s)^T\} \end{aligned} \quad (74)$$

j) FIM matrix with respect to \mathbf{p} and σ_n^2

$$\text{FIM}_{\mathbf{p}\sigma_n^2} = T \text{diag}^M(\mathbf{W}^H \mathbf{R}_s^{-2} \mathbf{W}) \quad (75)$$

k) FIM matrix with respect to \mathbf{p} and ν_l

$$\begin{aligned} \text{FIM}_{\mathbf{p}\nu_l} &= \\ &= 2T \Re\left\{ \left(\mathbf{W}^H \mathbf{R}_s^{-1} \mathbf{P}_{\mathbf{E}_l} \mathbf{A} \right) \odot \left(\mathbf{R}_s \mathbf{W}^H \mathbf{R}_s^{-1} \mathbf{W} \right)^T \right\} \end{aligned} \quad (76)$$

l) FIM matrix with respect to \mathbf{p} and η_l

$$\begin{aligned} \text{FIM}_{\mathbf{p}\eta_l} &= \\ &- 2T \Im\{(\mathbf{W}^H \mathbf{R}_s^{-1} \mathbf{P}_{\mathbf{E}_l} \mathbf{A}) \odot (\mathbf{R}_s \mathbf{W}^H \mathbf{R}_s^{-1} \mathbf{W})^T\} \end{aligned} \quad (77)$$

m) FIM matrix with respect to σ_n^2 and ν_l

$$\text{FIM}_{\sigma_n^2\nu_l} = 2T \text{diag}^M(\Re\{\mathbf{R}_s \mathbf{W}^H \mathbf{R}_s^{-2} \mathbf{P}_{\mathbf{E}_l} \mathbf{A}\})^T \quad (78)$$

n) FIM matrix with respect to σ_n^2 and η_l

$$\text{FIM}_{\sigma_n^2\eta_l} = -2T \text{diag}^M(\Im\{\mathbf{R}_s \mathbf{W}^H \mathbf{R}_s^{-2} \mathbf{P}_{\mathbf{E}_l} \mathbf{A}\})^T \quad (79)$$

o) FIM matrix with respect to ν_l and η_k

$$\begin{aligned} \text{FIM}_{\nu_l\eta_k} &= \\ &- 2T \Im\{(\mathbf{R}_s \mathbf{W}^H \mathbf{R}_s^{-1} \mathbf{P}_{\mathbf{E}_k} \mathbf{A}) \odot (\mathbf{R}_s \mathbf{W}^H \mathbf{R}_s^{-1} \mathbf{P}_{\mathbf{E}_l} \mathbf{A})^T \\ &+ (\mathbf{A}^H \mathbf{P}_{\mathbf{E}_l} \mathbf{R}_s^{-1} \mathbf{P}_{\mathbf{E}_k} \mathbf{A}) \odot (\mathbf{R}_s \mathbf{W}^H \mathbf{R}_s^{-1} \mathbf{W} \mathbf{R}_s)^T\} \end{aligned} \quad (80)$$

Since the general FIM is symmetric, the above expressions are exhaustive in describing the amount of information from all the model parameters embedded in the data. By taking the FIM inverse using (47), we have the CRLB for the DOAs. However, beyond yielding the CRLB for DOA estimates, these expressions can be used to calculate the CRLB for any parameter in the data model (1).

They can even be used for the calculus of the CRLB of the fully calibrated array if we set $L = 1$ and remove the rows and columns corresponding to the calibration parameters. Besides, they do not have any limitations with the quantity of sensors in

relation to the number of sources and consider the uncorrelated prior hypothesis for the sources, which is a core assumption for algorithms like GCA-MUSIC and GCA-rMUSIC.

VI. SIMULATION RESULTS AND DISCUSSION

In this section, we employ simulations to assess the algorithms' capabilities and demonstrate the applicability of the CRLB developed in this work. The performance curves are shown in terms of root mean squared-error (RMSE) in two distinct ways: comparison of the algorithms for a given geometry and comparison of the geometries for a given algorithm. All the results were obtained from an average of 50,000 simulation trials. In what follows, we outline the parameter setting, emphasizing that the number of signal sources surpasses the number of sensor elements within each subarray.

- Number of snapshots: $T = 2000$ (for the RMSE against SNR plots)
- Number of subarrays: $L = 2$
- SNR = 0 dB (for the RMSE against T plots)
- Type-II array with $N_l = 7$ sensors (total of $2N_l = 14$ sensors) and the following geometries for the reference subarray: a) II-MRA: $\mathbb{S}_l = \{0, 1, 4, 10, 12, 15, 17\}$; b) II-SNAQ2: $\mathbb{S}_l = \{0, 2, 3, 6, 9, 13, 14\}$; c) II-NAQ2: $\mathbb{S}_l = \{0, 1, 2, 3, 4, 9, 14\}$
- Normalized intersubarray displacement: $\mu = 8$, which implies that $\mathbf{h}(\theta_d) = [1, \exp(j\pi(\mu + \kappa)\theta_d)]^T$ corresponds to the vector of calibration parameters for $\theta_d = [\theta]_d$
- $D = 11$ sources with directions given by: $\theta = [\pm 0.75, \pm 0.6, \pm 0.45, \pm 0.3, \pm 0.15, 0]^T$

A. Analysis of degrees of freedom of full array and subarrays

In this section, we aim to characterize the weight function of the full array based on the weight function of the subarrays for Type II-MRA. To achieve this, we use the results from Theorem 1, derived in Section V-A. We observe that the intersubarray displacement is denoted by $\mu = 8$ and the aperture of each subarray is given by $\kappa = 17 - 0 = 17$. Additionally, the computation of the weight functions of the subarrays, as shown in the first two subplots of Fig. 2, indicates that the subarrays DoF and UDoF are equal to sDoF = UDoF = 35. Consequently, Theorem 1 dictates that the total DoF of the full array is given by

$$\begin{aligned} \text{DoF} &= L(\text{sDoF} - 1) + 2(L - 1)\mu + 1 \\ &= 2 \cdot (35 - 1) + 2(2 - 1)8 + 1 = 85 \end{aligned} \quad (81)$$

which agrees with the number of non-zero elements in the weight function of the entire array, as depicted in the fifth subplot of Fig. 2. It is also important to note also that this final weight function represents the sum of the first four weight functions. The weight functions shown in the third and fourth subplots are simply the weight functions of the subarrays translated by $\Delta = \pm(\mu + \kappa) = \pm 25$, as expected.

B. Computational complexity

The primary objective of GCA-(r)MUSIC is to perform DOA estimation when the number of sources is greater than that of sensors under two distinct scenarios: a) in fully calibrated arrays, where we advocate for non-coherent data processing to reduce hardware complexity and computational

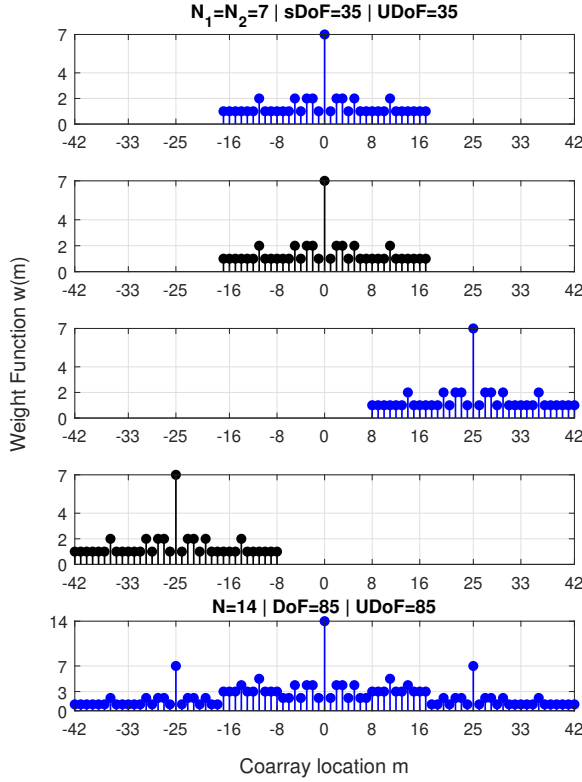


Fig. 2. Weight function of the full array as a result of the weight function of subarrays for II-MRA.

costs; and (b) in scenarios where calibration parameters remain unidentified, recommending the use of these algorithms to capitalize on their capability to estimate the DOAs with high performance, outperforming existing algorithms tailored for partially-calibrated scenarios. Regarding computational complexity, our approach is benchmarked in the first scenario against the SS-MUSIC (or coarray MUSIC) algorithm [3].

For the subsequent scenario, we draw a comparison with Spectral RARE and G-MUSIC, tailored for partially-calibrated arrays [5], [7]. Notably, while other algorithms in the literature address partially-calibrated arrays, they were excluded from our comparison due to their applicability solely to ULAs [24] or because their underlying signal model presupposes that the cross-covariance between subarrays is zero [13], a condition not applicable in our context.

In the subsequent simulation, we utilized a simulation server with 128 GB of RAM and an Intel Core i9-10980XE CPU at 3.0 GHz. The coding for all methods was optimally performed to minimize the number of required flops as much as possible. The normalized spacing between subarrays was assumed known for the SS-MUSIC algorithm (calibrated scenarios only) and unknown for the other four algorithms (GCA-(r)MUSIC, G-MUSIC and Spectral RARE). The spacing between subarrays constitutes our calibration information. The results concerning runtime, averaged over 50,000 simulation trials, are presented in Table II.

GCA-MUSIC and GCA-rMUSIC operate much faster than the other three methods. Moreover, G-MUSIC fails to identify the sources due to identifiability issues when the number of

TABLE II
RUNTIME OF GCA-(R)MUSIC AGAINST ESTABLISHED APPROACHES.

Algorithm	Runtime (Norm. Runtime)	DOA RMSE
GCA-rMUSIC	1.61 ms (1.00)	1.0943e-3
GCA-MUSIC	2.10 ms (1.306)	1.0954e-3
SS-MUSIC	12.15 ms (7.54)	0.15e-3
Spectral RARE	6.96 ms (4.32)	8.45e-3
G-MUSIC	2.45 ms (1.52)	0.99629

sources exceeds the number of sensors within a subarray. We also highlight that SS-MUSIC is approximately 12 times slower than the proposed approach and only can be used if all of the calibration parameters are known (in our case, the distance between subarrays). Despite those limitations, with a much higher computational and required hardware complexity, it provides the lowest RMSE because it does the processing using the calibration parameters, as expected. Among the algorithms designed for partially-calibrated scenarios, GCA-rMUSIC and GCA-MUSIC run approximately 4.3 and 3.3 times faster than Spectral MUSIC, respectively.

C. CRLB comparison

Regarding the CRLB, we consider five bounds:

- CRLB-FC: fully calibrated array without any special structure for the covariance matrix of the sources [25];
- CRLB-FC-UP: fully calibrated array assuming the sources are uncorrelated *a priori* - (*Uncorrelated Prior*), originally obtained in [26] and extended to deal with sparse arrays for the underdetermined case in [27]. It assumes the covariance matrix of the sources is diagonal;
- CRLB-PC: partially-calibrated array with covariance matrix of the sources without any special structure [7];
- CRLB-PC-UP-PROP**: partially-calibrated array assuming the sources are uncorrelated *a priori* (covariance matrix of the sources with diagonal structure), which is our *proposed bound*; and
- CRLB-PC-UxCov: partially-calibrated array assuming the cross-covariances between subarrays are zero-valued, i.e., the sources impinging on different subarrays are uncorrelated, proposed in [13].

The proposed CRLB-PC-UP-PROP bound is a unique contribution to the literature, providing a lower bound for the estimation performance of DOAs. This CRLB uniquely incorporates two critical assumptions: the uncorrelated nature of the sources, which is a fundamental consideration in coarray MUSIC algorithms, and the partial calibration of arrays. Unlike existing bounds such as CRLB-PC, CRLB-FC, and CRLB-PC-UxCov, the proposed bound overcomes numerical challenges encountered when the number of sources exceeds the number of sensors in the full array. This distinction not only underscores the practicality of our approach but also its applicability in scenarios often encountered in array signal processing.

The CRLBs above are depicted in Fig. 3. Among these bounds, it is evident that those assuming uncorrelated sources (appended by “-UP”), although initially lower, converge to the same value as its counterpart as the SNR increases. This convergence is observed in the pairs CRLB-FC/CRLB-FC-UP and CRLB-PC/CRLB-PC-UP-PROP. This phenomenon indicates that the uncertainty in the off-diagonal parameters

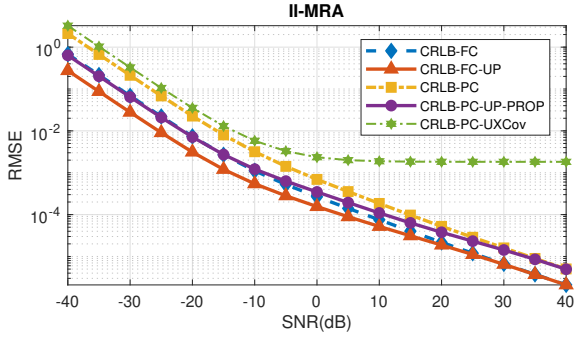


Fig. 3. CRLB curves against SNR for type-II MRA.

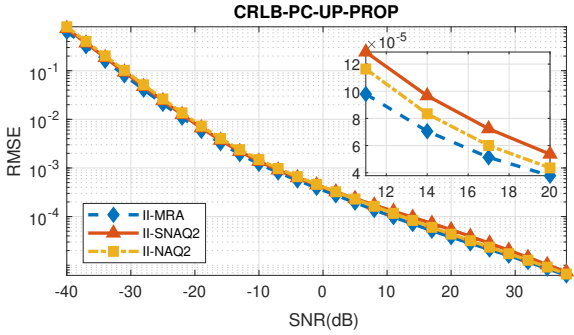


Fig. 4. Proposed CRLB-PC-UP-PROP against SNR for II-MRA, II-SNAQ2 and II-NAQ2.

of the sources' covariance matrix become negligible for the DOA estimation performance in substantially high SNR scenarios. Note that CRLB-PC-UP-PROP differs significantly from CRLB-PC for SNR values below 10 dB.

We also emphasize that CRLB-FC-UP is the bound with the lowest values, as it corresponds to a scenario with a fully calibrated array and uncorrelated sources, resulting in reduced uncertainty for DOA estimation algorithms. Lower uncertainty leads to better performance in estimation procedures. Moreover, we note that CRLB-PC-UXCov is the highest bound and, contrary to the other CRLB curves, it reaches a plateau after 10 dB. This behaviour, as expected and explained in [13], is due to the subarrays' covariance matrices not being full rank (i.e., more sources than sensors in each subarray). It is also important to mention that by employing the FIM expressions in Section V-D, we can estimate the CRLB for all parameters of the data model, not only the DOAs. This is because these matrices are explicitly provided, which extends the applicability of the work presented here to many parameter estimation algorithms.

In Fig. 4, we present a comparison of the three type-II array geometries in terms of the CRLB using CRLB-PC-UP-PROP. The curves, plotted against SNR, suggest that DOA estimation algorithms are likely to perform better with the type II-MRA geometry. This geometry consistently exhibits the lowest CRLB values. This theoretical aspect is corroborated by practical outcomes, as will be evidenced in Section VI-D. To allow a clearer comparison, we focused on the SNR range from 10 dB to 20 dB, displaying the curves in the right upper squared box in the figure.

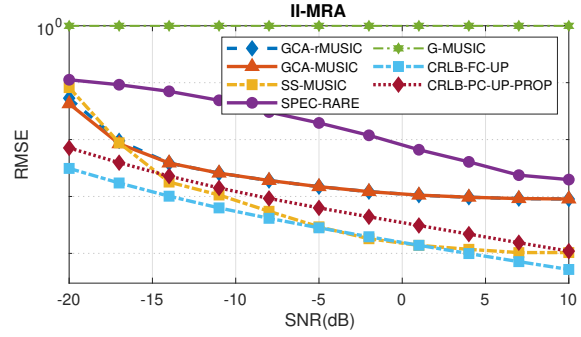


Fig. 5. Algorithm comparison. RMSE curves against SNR. GCA-MUSIC and GCA-rMUSIC for type-II arrays.

D. RMSE performance comparison

Before we enter into the RMSE discussion, it is worth exploring the expected RMSE for this scenario. Consider that a given estimation procedure obtains estimates of a random angle $\hat{\theta}_d$ from $(-1, 1]$. Additionally, suppose that this random variable follows a uniform distribution $\theta_d \sim \mathcal{U}(-1, 1)$. Then, the RMSE for this naive algorithm would be given by $\text{RMSE}^{\text{naive}} = \sqrt{\frac{1}{3} + \frac{1}{D} \sum_{d=1}^D \theta_d^2}$. Indeed, for this scenario we have $\text{RMSE}^{\text{naive}} = 0.7472$. Then, for an RMSE smaller than this, the estimator is better than a random choice for the DOAs. This is useful as a benchmark for the challenging scenarios in terms of data availability and SNR. Although it is not formally an upper bound on the estimator's RMSE, it is a metric we should pay attention to.

Next, we present the RMSE curves in Fig. 5, where the proposed algorithms are able to identify the sources in scenarios with more sources than sensors in each subarray and that GCA-rMUSIC slightly outperforms GCA-MUSIC for the lower SNR values. Although SS-MUSIC presents the best performance, it only applies to calibrated schemes, has a higher computational burden and we show its RMSE only for comparison purposes. The CRLB curve of our data model, as it was derived in Section V-D, CRLB-PC-UP-PROP shows that our algorithms get closer to optimum in the interval -17 dB up to -5 dB, saturating the performance as the SNR increases, which agrees with the analysis developed in the fully calibrated case for coarray MUSIC [11]. The RMSE value of 10^{-2} shows that Spectral RARE only achieves the performance of the proposed algorithms after the SNR increases by 15 dB. Additionally, we also observe that G-MUSIC fails to estimate the DOA of the sources because the number of sources exceeds the number of sensors in each subarray. Note that the optimization-based algorithms from [6] and [13] were excluded from our comparisons due to their significantly higher computational complexity—convex optimization iterative schemes without closed-form solutions for the former, and assumptions of zero-valued cross-covariance between subarrays for the latter. Moreover, these algorithms are based on data models that are different from the one used in this paper. Similar conclusions can be inferred from the RMSE curves versus the snapshots in Fig. 6.

In Fig. 7 and Fig. 8, we can verify that the performance varies largely with the geometry for both algorithms and that II-MRA presents the best estimation performance due to its larger number of DoF (virtual aperture), according to what was

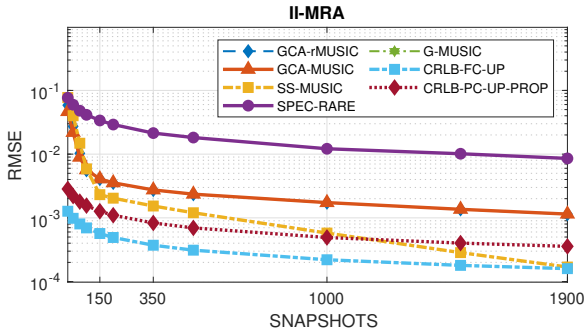


Fig. 6. Algorithm comparison. RMSE curves against SNAPSHOTS. GCA-MUSIC and GCA-rMUSIC for type-II arrays.

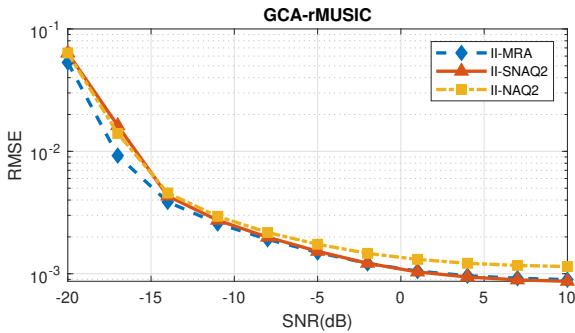


Fig. 7. Geometry comparison for GCA-root MUSIC. RMSE curves against SNR. Type-II MRA, NAQ2 and SNAQ2.

foreseen from the analysis of Fig. 4 in the previous section. The performance of II-MRA is achieved by II-SNAQ2 only after the thresholding of -5 dB for the SNR range.

VII. CONCLUSIONS

In this study, we have developed and analyzed novel design techniques for partially-calibrated sparse linear subarrays and introduced the algorithms GCA-MUSIC and GCA-rMUSIC for DOA estimation. These estimators effectively address the limitations of existing DOA estimation techniques, particularly in underdetermined scenarios where the number of sources exceeds the number of sensors. The proposed algorithms leverage the concept of sparse subarray design within the coarray domain to enhance estimation accuracy while maintaining computational efficiency. This approach not only expands the applicability of coarray-based signal processing to partially-calibrated arrays but also significantly increases the number

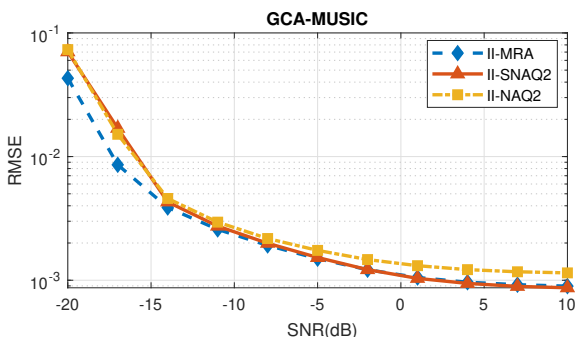


Fig. 8. Geometry comparison for GCA-MUSIC. RMSE curves against SNR. Type-II MRA, NAQ2 and SNAQ2.

of sources that can be estimated accurately. Through rigorous analysis, including the computation of the CRLB and extensive simulations, our methods have been shown to outperform existing approaches in terms of estimation precision and resource efficiency. This has the potential to impact various applications in sensor array processing by offering a more flexible and practical solution to the DOA estimation problem.

REFERENCES

- [1] H. L. Van Trees, *Optimum Array Processing*. New York, USA: John Wiley & Sons, Inc., 2002.
- [2] P. Pal and P. P. Vaidyanathan, "Nested arrays: A novel approach to array processing with enhanced degrees of freedom," *IEEE Transactions on Signal Processing*, vol. 58, no. 8, pp. 4167–4181, 2010.
- [3] —, "A novel array structure for directions-of-arrival estimation with increased degrees of freedom," in *2010 IEEE International Conference on Acoustics, Speech and Signal Processing*, no. 2. IEEE, 2010, pp. 2606–2609.
- [4] C.-L. Liu and P. P. Vaidyanathan, "Super Nested Arrays: Linear Sparse Arrays With Reduced Mutual Coupling—Part I: Fundamentals," *IEEE Transactions on Signal Processing*, vol. 64, no. 15, pp. 3997–4012, aug 2016.
- [5] D. Rieken and D. Fuhrmann, "Generalizing MUSIC and MVDR for multiple noncoherent arrays," *IEEE Transactions on Signal Processing*, vol. 52, pp. 2396–2406, 9 2004.
- [6] T. Tirer and O. Bialer, "A method for reducing the performance gap between non-coherent and coherent sub-arrays," *IEEE Transactions on Signal Processing*, vol. 68, pp. 3358–3370, 2020.
- [7] C. See and A. Gershman, "Direction-of-arrival estimation in partly calibrated subarray-based sensor arrays," *IEEE Transactions on Signal Processing*, vol. 52, pp. 329–338, 2004.
- [8] T. Tirer and O. Bialer, "Direction of arrival estimation for non-coherent sub-arrays via joint sparse and low-rank signal recovery." *IEEE*, 6 2021, pp. 4395–4399.
- [9] D. Malioutov, M. Cetin, and A. S. Willsky, "A sparse signal reconstruction perspective for source localization with sensor arrays," *IEEE Transactions on Signal Processing*, vol. 53, no. 8, pp. 3010–3022, 2005.
- [10] W. K. Ma, T. H. Hsieh, and C. Y. Chi, "Doa estimation of quasi-stationary signals via khatri-rao subspace," *ICASSP, IEEE International Conference on Acoustics, Speech and Signal Processing - Proceedings*, pp. 2165–2168, 2009.
- [11] M. Wang and A. Nehorai, "Coarrays, music, and the cramér-rao bound," *IEEE Transactions on Signal Processing*, vol. 65, no. 4, pp. 933–946, 2017.
- [12] C. Steffens and M. Pesavento, "Block- and rank-sparse recovery for direction finding in partly calibrated arrays," *IEEE Transactions on Signal Processing*, vol. 66, no. 2, pp. 384–399, 2018.
- [13] W. Suleiman, P. Parvazi, M. Pesavento, and A. M. Zoubir, "Non-coherent direction-of-arrival estimation using partly calibrated arrays," *IEEE Transactions on Signal Processing*, vol. 66, no. 21, pp. 5776–5788, 2018.
- [14] W. S. Leite and R. C. de Lamare, "Noncoherent sparse subarrays for DOA estimation based on low-rank and sparse recovery," in *30th European Signal Processing Conference (EUSIPCO)*, 2022.
- [15] —, "Partially-calibrated sparse subarrays for direction-of-arrival estimation with increased degrees of freedom," in *56th Asilomar Conference on Signals, Systems, and Computers*, 2022.
- [16] A. Swindlehurst, P. Stoica, and M. Jansson, "Exploiting arrays with multiple invariances using music and mode," *IEEE Transactions on Signal Processing*, vol. 49, pp. 2511–2521, 2001.
- [17] A. Moffet, "Minimum-redundancy linear arrays," *IEEE Transactions on Antennas and Propagation*, vol. 16, no. 2, pp. 172–175, 1968.
- [18] D.-Z. Feng, W. X. Zheng, and A. Cichocki, "Matrix-group algorithm via improved whitening process for extracting statistically independent sources from array signals," *IEEE Transactions on Signal Processing*, vol. 55, pp. 962–977, 3 2007.
- [19] W. Xia and Z. He, "Active direction finding in imaging sensor nets," in *11th IEEE Singapore International Conference on Communication Systems*. IEEE, 2008, pp. 1359–1363.
- [20] A. Barabell, "Improving the resolution performance of eigenstructure-based direction-finding algorithms," in *IEEE International Conference on Acoustics, Speech, and Signal Processing (ICASSP)*, vol. 8. IEEE, 1983, pp. 336–339.
- [21] S. Al-Juboori and X. N. Fernando, "Multiantenna spectrum sensing over correlated nakagami- m channels with mrc and egc diversity receptions," *IEEE Transactions on Vehicular Technology*, vol. 67, no. 3, pp. 2155–2164, 2018.

- [22] W. S. Leite and R. C. de Lamare, "List-Based OMP and an Enhanced Model for DOA Estimation With Nonuniform Arrays," *IEEE Transactions on Aerospace and Electronic Systems*, vol. 57, no. 6, pp. 4457–4464, 2021.
- [23] G. H. Golub and C. F. V. Loan, *Matrix Computations*, 4th ed. Johns Hopkins University Press, 2012.
- [24] W. Suleiman and P. Parvazi, "Search-free decentralized direction-of-arrival estimation using common roots for non-coherent partly calibrated arrays," in *International Conference on Acoustics, Speech and Signal Processing (ICASSP)*. IEEE, 2014, pp. 2292–2296.
- [25] P. Stoica and A. Nehorai, "MUSIC, maximum likelihood, and Cramer-Rao bound," *IEEE Transactions on Acoustics, Speech, and Signal Processing*, vol. 37, pp. 720–741, 1989.
- [26] M. Jansson, B. Göransson, and B. Ottersten, "A subspace method for direction of arrival estimation of uncorrelated emitter signals," *IEEE Transactions on Signal Processing*, vol. 47, 1999.
- [27] C.-L. Liu and P. Vaidyanathan, "Cramér–Rao bounds for coprime and other sparse arrays, which find more sources than sensors," *Digital Signal Processing*, vol. 61, pp. 43–61, 2017.



Wesley S. Leite was born in Guarulhos, Brazil, in 1991. He received the B.E. degree in electrical engineering from the Federal University of Maranhão (UFMA), São Luís, in 2014, and the M.S. degree in electrical engineering from the Pontifical Catholic University of Rio de Janeiro (PUC-Rio), Rio de Janeiro, 2020. He is currently pursuing the Ph.D. degree in the field of signal processing at PUC-Rio. His main research interests include sensor array signal processing for beamforming and direction-of-arrival (DOA) estimation.



Rodrigo C. de Lamare was born in Rio de Janeiro, Brazil, in 1975. He received his Diploma in electronic engineering from the Federal University of Rio de Janeiro in 1998 and the MSc and PhD degrees in electrical engineering from the Pontifical Catholic University of Rio de Janeiro (PUC-Rio) in 2001 and 2004, respectively. Since January 2006, he has been with the Communications Group, School of Physics, Engineering and Technology, University of York, United Kingdom, where he is a Professor. Since April 2013, he has also been a Professor at PUC-Rio.

Dr de Lamare is a senior member of the IEEE and an elected member of the IEEE Signal Processing for Communications and Networking Committee and the IEEE Sensor Array and Multichannel Signal Processing. He served as editor for IEEE Wireless Communications Letters and IEEE Transactions on Communications, and is currently an associate editor of IEEE Transactions on Signal Processing. His research interests lie in communications and signal processing, areas in which he has published over 500 papers in international journals and conferences.



Yuriy Zakharov (M'01 - SM'08) received the M.Sc. and Ph.D. degrees in electrical engineering from the Power Engineering Institute, Moscow, Russia, in 1977 and 1983, respectively. From 1977 to 1983, he was with the Special Design Agency in the Moscow Power Engineering Institute. From 1983 to 1999, he was with the N. N. Andreev Acoustics Institute, Moscow. From 1994 to 1999, he was with Nortel as a DSP Group Leader. Since 1999, he has been with the University of York, UK, where he is currently a Reader in the School of Physics, Engineering and

Technology. His research interests include signal processing, communications, and underwater acoustics.



Wei Liu (S'01-M'04-SM'10) received his BSc (Space Physics) and LLB (Intellectual Property Law) degrees from Peking University, China, in 1996 and 1997, respectively, MPhil from the Department of Electrical and Electronic Engineering, University of Hong Kong in 2001, and PhD from the School of Electronics and Computer Science, University of Southampton, UK, in 2003. He then worked as a postdoc first at Southampton and later at Imperial College London. From 2005 to 2023, he was a Lecturer/Senior Lecturer at the Department of Electronic and Electrical Engineering, University of Sheffield, UK and from 2023 to 2024, a Reader at the School of Electronic Engineering and Computer Science, Queen Mary University of London. Since 2024, he has been a Professor at the Department of Electrical and Electronic Engineering, Hong Kong Polytechnic University. He has published 430+ journal and conference papers, six book chapters, and two research monographs titled "Wideband Beamforming: Concepts and Techniques" (Wiley, 2010) and "Low-Cost Smart Antennas" (Wiley, 2019), respectively. His research interests cover a wide range of topics in signal processing, with a focus on sensor array signal processing and its various applications, such as robotics and autonomous systems, human computer interface, radar, sonar, and wireless communications.



Martin Haardt (Fellow, IEEE) received the Diplom-Ingenieur (M.S.) degree in electrical engineering from the Ruhr-University Bochum, Germany, in 1991 and the Doktor-Ingenieur (Ph.D.) degree from Munich University of Technology, Germany, in 1996. During his diploma studies he also studied as a visiting scholar at Purdue University, USA. Since 2001, he has been a Full Professor in the Department of Electrical Engineering and Information Technology and Head of the Communications Research Laboratory at Ilmenau University

of Technology, Germany. In 1997 he joined Siemens Mobile Networks in Munich, Germany, where he was responsible for strategic research for third generation mobile radio systems. From 1998 to 2001 he was the Director for International Projects and University Cooperations in the mobile infrastructure business of Siemens in Munich, where his work focused on mobile communications beyond the third generation. Martin Haardt is a EURASIP fellow. He received the 2009 Best Paper Award from the IEEE Signal Processing Society, the Vodafone Innovations Award for outstanding research in mobile communications, the ITG best paper award from the Association of Electrical Engineering, Electronics, and Information Technology (VDE), and the Rohde & Schwarz Outstanding Dissertation Award. His research interests include wireless communications, array signal processing, high-resolution parameter estimation, as well as tensor-based signal processing. Prof. Haardt has served as a Senior Editor for the IEEE Journal of Selected Topics in Signal Processing (since 2019), as an Associate Editor for the IEEE Transactions on Signal Processing (2002-2006 and 2011-2015), the IEEE Signal Processing Letters (2006-2010), the Research Letters in Signal Processing (2007-2009), the Hindawi Journal of Electrical and Computer Engineering (since 2009), the EURASIP Signal Processing Journal (2011-2014), and as a guest editor for the EURASIP Journal on Wireless Communications and Networking. From 2011 until 2019 he was an elected member of the Sensor Array and Multichannel (SAM) technical committee of the IEEE Signal Processing Society, where he served as the Vice Chair (2015 – 2016), Chair (2017 – 2018), and Past Chair (2019). Since 2020, he has been an elected member of the Signal Processing Theory and Methods (SPTM) technical committee of the IEEE Signal Processing Society. Moreover, he has served as the technical co-chair of PIMRC 2005 in Berlin, Germany, ISWCS 2010 in York, UK, the European Wireless 2014 in Barcelona, Spain, the Asilomar Conference on Signals, Systems, and Computers 2018, USA, as well as ISWCS 2024 in Rio de Janeiro and as the general co-chair of WSA 2013 in Stuttgart, Germany, ISWCS 2013 in Ilmenau, Germany, CAMSAP 2013 in Saint Martin, French Antilles, WSA 2015 in Ilmenau, SAM 2016 in Rio de Janeiro, Brazil, CAMSAP 2017 in Curacao, Dutch Antilles, SAM 2020 in Hangzhou, China, the Asilomar Conference on Signals, Systems, and Computers 2021, USA, as well as CAMSAP 2023 in Costa Rica.